DNA damage and somatic mutations in mammalian cells after irradiation with a nail polish dryer

Maria Zhivagui[1-3], Areebah Hoda[1], Noelia Valenzuela[3], Yi-Yu Yeh[2], Jason Dai[2], Yudou He[1-3], Shuvro P. Nandi[1-3], Burcak Otlu[1-3], Bennett Van Houten[4], and Ludmil B. Alexandrov[1-3*]

Affiliations

[1]Department of Cellular and Molecular Medicine, UC San Diego, La Jolla, CA, 92093, USA

[2]Department of Bioengineering, UC San Diego, La Jolla, CA, 92093, USA

[3]Moores Cancer Center, UC San Diego, La Jolla, CA, 92037, USA

[4]UPMC-Hillman Cancer Center, University of Pittsburgh, PA 15213

[*]Correspondence should be addressed to L2alexandrov@health.ucsd.edu.

ABSTRACT

Ultraviolet A light is commonly emitted by UV-nail polish dryers with recent reports suggesting that long-term use may increase the risk for developing skin cancer. However, no experimental evaluation has been conducted to reveal the effect of radiation emitted by UV-nail polish dryers on mammalian cells. Here, we show that irradiation by a UV-nail polish dryer causes high levels of reactive oxygen species, consistent with 8-oxo-7,8-dihydroguanine damage and mitochondrial dysfunction. Analysis of somatic mutations reveals a dose-dependent increase of C:G>A:T substitutions in irradiated samples with mutagenic patterns similar to mutational signatures attributed to reactive oxygen species. In summary, this study demonstrates that radiation emitted by UV-nail polish dryers can both damage DNA and permanently engrave mutations on the genomes of mammalian cells. These results have far-reaching implications in regard to public health and to preventing skin cancer due to consumer-based exposure to ultraviolet light from artificial sources.

34 **INTRODUCTION**

35 Ultraviolet (UV) light is a type of electromagnetic radiation with a wavelength ranging between
36 10nm and 400nm. Since wavelengths below 280nm are generally blocked by the Earth's
37 stratospheric ozone, the UV light that reaches the Earth's surface is between 280nm and 400nm[1].
38 The UV spectrum can be further categorized based on its effect on human skin as well as on its
39 ability to induce DNA damage[2]. Ultraviolet B light (UVB; 280-315nm) accounts for about 10%
40 of the UV found on Earth, penetrates the outer layer of the skin, and it induces a plethora of DNA
41 lesions including cyclobutane-pyrimidine dimers and 6-4 photoproducts[3,4]. In contrast, ultraviolet
42 A light (UVA; 315-400nm) constitutes approximately 90% of the ultraviolet radiation that reaches
43 the surface of the Earth, it can penetrate the skin more deeply, and it causes little direct DNA
44 damage as UVA is poorly absorbed by DNA[2,5-12].

45

46 The International Agency for Research on Cancer has classified broadband UVA (315-400nm) as
47 a Group 1 carcinogen, based on sufficient evidence for carcinogenicity in both humans and
48 experimental models combined with strong mechanistic considerations[13]. While UVA is found in
49 sunlight, most of UVA environmental toxicity has been attributed to the use of commercial
50 products, such as tanning beds[14]. Consistently, meta-analyses have shown a causal relation
51 between skin cancer and irradiation with UV-emitting tanning devices[13,15]. Further, it has been
52 demonstrated that skin squamous-cell carcinoma will develop in mice after long-term exposure to
53 broadband UVA[16-19]. Prior experimental studies have also suggested that UVA irradiation leads to
54 indirect DNA damage mostly through the accumulation of 8-oxo-7,8-dihydro-2′-deoxyguanosine
55 (8-oxo-dG) derived from reactive oxygen species[20-24]. Studies using reporter single-gene assays
56 have identified an enrichment of C:G>A:T mutations in UVA irradiated samples consistent with

57 damage due to 8-oxo-dG[25-28]. Despite prior evidence for carcinogenicity of broadband UVA (315-
58 400nm), UVA radiation in subsets of this spectrum is widely used in a surfeit of consumer products
59 without extensive evaluation of the potential carcinogenic and mutagenic effects of these products.
60 One prominent example is UV-nail polish dryers, which have become increasingly popular in the
61 last decade[29,30].
62
63 UV-nail lamps are used to cure and dry nail polish formulas, known as gels, which are oligomers
64 requiring exposure to UV radiation to harden into polymers. These UV-gel nail devices release
65 UVA radiation with either very little or, in most cases, no UVB radiation[31]. UV-gel nail devices
66 contain multiple bulbs, emitting UV wavelengths between 340 and 395nm that can react and
67 activate the photo-initiators in a gel[29]. Concerns have been raised regarding the magnitude of DNA
68 damage that can be posed from exposure to UV-nail machines and their potential role in skin
69 carcinogenesis[30,32]. Notably, in most cases, both nails and hands are irradiated up to 10 minutes
70 with a UV-nail dryer per session[32]. The number of nail salon clients is estimated to reach 8 clients
71 a day per nail technician, accounting for approximately 3 million daily clients in the United
72 States[33]. Typically, regular users change their gel manicures every 2 weeks[32]. Recently, a small
73 number of melanoma and non-melanoma cases, reported either on the nail or on the dorsum of the
74 hand, have also been putatively attributed to exposure to UV radiation emitted by nail polish
75 dryers[32,34].
76
77 In this work, we perform an *in vitro* irradiation of human and murine cells using distinct acute and
78 chronic exposure protocols to evaluate the DNA damage and mutagenic effects of ultraviolet
79 radiation emitted by a nail polish UV-dryer. Irradiated and control cells are subjected to multiple

80 assays for measuring DNA damage as well as to DNA sequencing either by bulk whole-genome
81 sequencing after clonal expansion or by single-molecule duplex sequencing without clonal
82 expansion (**Figure 1**). Elevated levels of reactive oxygen species (ROS) are observed in UV-
83 irradiated samples, consistent with 8-oxo-dG damage and mitochondrial dysfunction. Analysis of
84 somatic mutations reveals a dose-dependent increase of C:G>A:T mutations in irradiated samples
85 with patterns similar to the ones of COSMIC signatures SBS18/36, which were previously
86 attributed to oxidative damage[35-37]. Finally, re-examination of previously generated skin cancers
87 uncovers that SBS18/36 are ubiquitously present in melanoma and account for ~12% of the
88 previously annotated driver mutations. Our results provide a comprehensive profile of the DNA
89 damage and somatic mutations in mammalian cells after irradiation with a nail polish dryer.
90

91 **RESULTS**

92 **Experimental Design and Examination of Cytotoxicity**

93 To study the cytotoxic effect of irradiation by a UV-nail polish dryer, mouse embryonic fibroblasts
94 (MEFs), human foreskin fibroblasts (HFFs), and adult human epidermal keratinocytes (HEKa)
95 were exposed under several distinct conditions (**Figure 1**). Each primary cell line was irradiated
96 one, two, or three times, with the duration of each exposure lasting between 0 and 20 minutes. Cell
97 viability was measured 48 hours after the final irradiation with each condition repeated at least
98 three times. Analysis of cell viability revealed that UV radiation induced cytotoxicity with higher
99 number of exposures causing a lower cell viability (**Figure 2*a***). For example, in all cell line
100 models, a single 20-minute irradiation resulted in 20% to 30% cell death, while three consecutive
101 20-minute exposures caused between 65% and 70% cell death (q-values < 0.05; Mann-Whitney U
102 tests; **Figure 2*a***).

103

104 Assessment of DNA damage was performed on MEFs and HFFs after either two 20-minute
105 irradiations taking place within 2 hours in a single day (termed, acute exposure; **Figure 1*a***;
106 **Supplementary Table 1**) or after three 20-minute irradiations each occurring in 3 consecutive
107 days (termed, chronic exposure; **Figure 1*a***; **Supplementary Table 1**). Assessment of DNA
108 damage was also performed at the same timepoint for unexposed MEF and HFF cells. Moreover,
109 to assess the presence of somatic mutations, both irradiated and control cells were subjected to
110 barrier bypass-clonal expansion[38], grown for the same number of doubling populations, and
111 subjected to bulk whole-genome sequencing (**Supplementary Table 1**; **Supplementary Figure**
112 **1**). Specifically, irradiated and control MEF cells were grown for ~28 doubling populations prior

113 to bulk whole-genome sequencing, while exposed and unexposed HFF cells were grown for ~35
114 rounds of cell division (**Supplementary Table 1**; **Supplementary Figure 1**).
115
116 In the case of HEKa, cells were only chronically exposed with three 20-minute irradiations each
117 occurring in 3 consecutive days (**Figure 1*b***). Assessment of DNA damage in HFFs was conducted
118 similarly to the assessments perform for MEFs and HFFs (**Supplementary Table 1**). Nevertheless,
119 somatic mutations in HEKa cells were detected using an orthogonal approach to the one applied
120 for MEFs and HFFs by avoiding barrier bypass-clonal expansion. Specifically, irradiated and
121 control HEKa cells were grown for exactly 14 days (**Figure 1*b***), corresponding to approximately
122 8 doubling populations, and were subsequently subjected to targeted single-molecule duplex
123 sequencing[39].
124
125 **Quantification of Genotoxicity**
126 Genotoxicity of mammalian cells irradiated with a UV-nail polish dryer was evaluated 4 hours
127 after exposure using γH2Ax immunofluorescence[40]. Statistically significant increases in the
128 number of γH2Ax foci were observed when comparing irradiated MEF, HFF, and HEKa to control
129 cells for all cell lines as well as for all types of exposure (**Figure 2*b-e***). For MEFs, the number of
130 γH2Ax foci increased 186-fold for acute exposure when compared to control samples (q-value:
131 3.6×10^{-4}; Mann-Whitney U test) and 183.3-fold for chronic exposure (q-value: 2.5×10^{-4}; **Figure**
132 **2*c***). Acutely exposed HFFs had 154.7-fold elevation of the number of γH2Ax foci when compared
133 to control samples (q-value: 3.6×10^{-4}), while chronically exposed HFFs exhibited 137-fold
134 elevation (q-value: 1.2×10^{-5}; **Figure 2*d***). Similarly, irradiated HEKa cells showed a significant

135 increase of γH2Ax foci when compared to control samples with 398-fold elevation for acute
136 exposure (q-value: 3 x 10^{-9}) and 260-fold for chronic exposure (q-value: 2 x 10^{-9}; **Figure 2*e***).
137
138 **Evaluation of Photoproducts' Formation**
139 Immunofluorescence was used to evaluate whether irradiation from a UV-nail dryer resulted in the
140 formation of cyclobutane pyrimidine dimers (CPDs) or pyrimidine-pyrimidone (6-4) photoproduct
141 (6-4PPs) in all cell lines models after either acute or chronic exposure (**Supplementary Figure 2**).
142 As a positive control, each cell line model was also exposed to ultraviolet C light (UVC), which is
143 known to form these photoproducts[41]. Our results demonstrated that, in contrast to UVC radiation,
144 UV emitted by a nail-polish dryer induced neither CPDs nor 6-4PPs in any of the exposed cell
145 lines (**Supplementary Figure 2**).
146
147 **Quantification of Oxidative Damage**
148 To evaluate oxidative damage after irradiation, we utilized three independent *in vitro* assays,
149 including: *(i)* CellROX for detection of oxidative stress[42]; *(ii)* enzyme-linked immunosorbent assay
150 (ELISA) for quantification of 8-oxo-dG[43,44]; and *(iii)* OxiSelect™ for detection of cytosolic and
151 extra-cellular reactive oxygen species (ROS)[45].
152
153 CellROX green is a fluorogenic probe used for measuring oxidative stress in live cells, namely
154 superoxide radical anion ($O_2^{\bullet}$) and hydroxyl radical (•OH)[42]. The reduced state of the CellROX
155 dye is weakly fluorescent inside cells but once oxidized by ROS, the dye binds to nucleic acids in
156 cells and exhibits bright green photostable fluorescence[42]. The three cell models (MEF, HFF, and
157 HEKa) were tested using CellROX green dye immediately after irradiation (**Supplementary**
158 **Table 1**). Live cell imaging results unveiled a clear increase of CellROX green fluorescence in

159 irradiated cells compared to controls in all cases (**Figure 3*a-b***). To ensure that the CellROX
160 fluorescence is due to ROS formation in the cells, we further challenged the HEKa cells with a
161 ROS scavenger, namely N-acetyl-L-cysteine (NAC), prior to irradiation[46]. Quantification of the
162 number of CellROX foci without NAC treatment revealed a significant increase of oxidative stress
163 in irradiated HEKa cells when compared to the controls (5.5-fold increase for acute, q-value < 2.2
164 x 10^{-16}; 4.4-fold increase for chronic, q-value < 2.2 x 10^{-16}; Mann-Whitney U tests). Importantly,
165 the number of CellROX foci significantly decreased after NAC treatment when compared to
166 untreated cells (acute: 5.2-fold decrease, q-value= 2 x 10^{-3}; chronic: 4.2-fold decrease, q-value=
167 1.4 x 10^{-3}), confirming that irradiation by a nail polish dryer is responsible for oxidative stress
168 induction in mammalian cells.
169
170 ELISA quantifications of 8-oxo-dG were performed for all cell line modes in 3 distinct timepoints:
171 *(i)* immediately after exposure; *(ii)* 4 hours post-irradiation; and *(iii)* 24 hours post-irradiation
172 (**Figure 3*c-e***). Additionally, three positive controls, namely, hydrogen peroxide (H_2O_2), ultraviolet
173 C radiation (UVC), and potassium bromate ($KBrO_3$), were also evaluated for each of the cell lines
174 immediately after exposure (**Figure 3*c-e***). Overall, statistically significant enrichments of 8-oxo-
175 dG concentrations, ranging from 5- to 20-fold (q-values < 0.05), were observed in irradiated cells
176 when compared to the control cells for all cell line models and for all exposure types (**Figure 3*c-***
177 ***e***). In all cases, this level of enrichment was comparable or higher to the one exhibited by the
178 exposure to positive controls. Moreover, the amount of 8-oxo-dG remained stable even 24 hours
179 after irradiation (**Figure 3*c-e***). These results confirm that irradiation by a UV-nail polish dryer
180 causes high levels of oxidative stress mediated by ROS formation and subsequent oxidation of
181 DNA bases via 8-oxo-dG formation.

182

183 To further evaluate the total free radicals in the irradiated MEF and HFF cells, we utilized
184 OxiSelect™ *In Vitro* ROS/RNS Assay Kit. This assay employs a proprietary quenched fluorogenic
185 probe, dichlorodihydrofluorescin DiOxyQ (DCFH-DiOxyQ), which is newly developed derivative
186 of DCFDA and has been shown to be more specific for the detection of ROS/RNS[45,47,48]. Cytosolic
187 and extra-cellular ROS signals were evaluated in MEF and HFF samples, in three different
188 timepoints: *(i)* immediately after exposure, *(ii)* 20 minutes post-irradiation, and *(iii)* 24 hours post-
189 irradiation. (**Supplementary Figure 3**). ROS-induced florescence was elevated in both acutely
190 and chronically exposed mammalian cells compared to the untreated cells. For both MEFs and
191 HFFs, acute exposure resulted in 2- to 8-fold increase of both cytosolic and extra-cellular ROS
192 compared to their respective controls (q-values: 2×10^{-5} and 1.7×10^{-6} for MEF cytosolic and
193 extracellular, respectively; q-values: 2×10^{-3} and 3×10^{-5} for HFF cytosolic and extracellular,
194 respectively; Mann-Whitney U tests; **Supplementary Figure 3**).

195

196 **Examining Mitochondrial Membrane Potential and ROS Generation**

197 As mitochondria are particularly sensitive to excessive ROS generated by UV radiation and they
198 play key role in oxidants production[49,50], we also examined mitochondrial potential membrane and
199 evaluated the mitochondrial ROS production after irradiation with a UV-nail polish dryer.
200 Mitochondrial activity and functionality were conducted in all three cellular models 24 hours post-
201 irradiation by using a tetramethylrhodamine dye (TMRM), which is taken up by mitochondria with
202 a high proton gradient and is a measure of well coupled mitochondria (**Figure 4*a***; **Supplementary**
203 **Figure 4**). In all three cellular models, irradiation resulted in reduced TMRM fluorescence
204 indicating a likely mitochondrial loss of mitochondrial membrane potential (**Figure 4*a***;

205 **Supplementary Figure 4**). Moreover, MitoSOX red mitochondrial superoxide indicator dye was
206 applied to HEKa cells 24 hours post-radiation. MitoSOX selectively targets the mitochondria and,
207 after being oxidized by superoxide, it produces red fluorescence upon binding to nucleic acid in
208 the cells. Live cell imaging of acutely and chronically irradiated HEKa cells revealed MitoSOX
209 red fluorescence when compared to unexposed HEKa controls (**Figure 4*b***). Quantification of the
210 number of MitoSOX foci per cell revealed a significant increase of oxidative stress in mitochondria
211 of irradiated HEKa cells when compared to the controls (8.3-fold increase for acute, q-value: 7.4
212 x 10^{-12}; 17-fold increase for chronic, q-value < 3.6 x 10^{-10}; Mann-Whitney U tests; **Figure 4*c***).
213 This increase in MitoSOX fluorescence putatively suggests an elevation of oxidative stress in
214 mitochondria caused by irradiation. In principle, some forms of ROS intermediates cannot persist
215 in the cell and the observed increase of oxidative stress in the mitochondria could be due to cellular
216 damage leading to chronic and persistent state of hydrogen peroxide production that may cause
217 oxidation of nuclear proteins over a 24-hour period[51]. Taken altogether, these data suggest that
218 UVA light can cause mitochondrially generated ROS and persistent nuclear DNA damage.
219 Nevertheless, other explanations of the observed increase of oxidative stress in the mitochondria
220 are also possible.
221

222 **Somatic Mutations After Barrier Bypass-clonal Expansion**

223 To evaluate the somatic mutations engraved by UV radiation from a nail dryer, we utilized two
224 orthogonal sequencing approach: *(i)* bulk whole-genome sequencing of immortalized HFF and
225 MEF clones, grown for the same number of doubling populations after barrier bypass-clonal
226 expansion (**Supplementary Figure 1**); and *(ii)* single molecule duplex sequencing for HEKa cells
227 without clonal expansion (**Figure 1*b***). A total of 15 HFF and 15 MEF immortalized clones were

228 subjected to bulk whole-genome sequencing (WGS) at 30x coverage, including: *(i)* 5 HFF and 5
229 MEF clones after acute irradiation; *(ii)* 5 HFF and 5 MEF clones after chronic irradiation; *(iii)* 5
230 HFF and 5 MEF unirradiated control clones. Somatic mutations were derived for immortalized
231 clones by comparing the WGS data of each immortalized clone to the WGS data from the
232 respective primary cell line using previously established state-of-the-art bioinformatics pipelines
233 (**Figure 1**; **Supplementary Figure 5**). Examining the variant allele frequencies (VAFs) for single
234 base substitutions revealed that the majority of MEF mutations are subclonal with a mean VAF of
235 approximately 0.25, while most HFF mutations are clonal with a mean VAF of approximately 0.50
236 (**Supplementary Figure 6*a-b***). These results are consistent with previous observations in these
237 model systems[38,52] and they reflect experimental differences between the murine and human cell
238 line models after clonal expansion. Specifically, MEFs undergoing barrier-bypass clonal
239 expansion are most likely to yield two subclonal populations[38,52], while HFFs undergoing single-
240 cell subcloning have a high propensity for selecting a single clone[38].
241
242 Single base substitutions (SBSs) were 2- and 2.5-fold elevated in acutely and chronically irradiate
243 MEF cells, respectively, when compared to control cells (q-values<0.01; Mann-Whitney U tests;
244 **Figure 5*a***). Stratification of SBSs based on their simplest six channel classification (*i.e.*, C>A,
245 C>G, C>T, T>A, T>C, T>G; each mutation referred to by the pyrimidine base of the Watson-
246 Crick DNA base-pair) revealed a significant increase of C>A transversions in acute and chronic
247 MEFs exposed to UV emitted from a nail dryer: 2.8- and 4.2-fold increase for acute and chronic,
248 respectively (q-values: 0.02 and 0.016; Mann-Whitney U tests; **Figure 5*b***). Importantly, the
249 number of C>A single base substitutions found in MEF clones was positively correlated with the
250 number of UV exposures (**Figure 5*c***; Spearman's rank correlation: 0.64; p-value: 0.0098).

251

252 Immortalized HFF clones exhibited similar behaviors to the ones of MEF clones, albeit, in most
253 cases, with smaller effect sizes. Specifically, substitutions were 1.2- and 1.4-fold enriched in
254 acutely and chronically irradiated HFF cells compared to control cells (q-values<0.01; Mann-
255 Whitney U tests; **Figure 5*a***). An elevation of C>A mutations was also observed in acutely
256 irradiated HFF clones (1.22-fold increase with q-value: 0.015; Mann-Whitney U tests; **Figure 5*b***)
257 as well as in chronically irradiated HFF clones (1.63-fold increase with q-value: 7.9×10^{-3}; Mann-
258 Whitney U tests; **Figure 5*b***). Similarly, the number of C>A transversions exhibited a positive
259 correlation with the number of UV exposures in HFFs (**Figure 5*c***; Spearman's rank correlation:
260 0.85; p-value: 5.9×10^{-5}).

261

262 Analysis of somatic copy number changes revealed that all HFF samples are almost perfectly
263 diploid with the exception of one chronically exposed HFF sample, which showed loss of
264 heterozygosity in several large chromosomes. Consistent with prior reports[38,52], focal copy-number
265 changes were found in some of the spontaneous and irradiated MEF samples, which may lead to
266 an inaccurate estimation of the mutational burden caused by genomic instability in MEFs.
267 Specifically, four of the MEF samples were found to have high number of somatic copy-number
268 changes with evidence for potential whole-genome doubling followed by loss of heterozygosity.
269 These four MEF samples included: one spontaneous, one acutely irradiated, and two chronically
270 irradiated clones. Nevertheless, no statistically significant differences in overall somatic copy
271 number changes or in overall ploidy were observed between the irradiated and the control cells for
272 any of the utilized cell line models. Further, no differences in the numbers of small insertions or

273 deletions were observed between the irradiated and the control cells for any of the used cell line
274 models (**Figure 5*d***).
275
276 **Somatic Mutations After Duplex Sequencing**
277 In principle, detection of somatic mutations in experimental systems requires clonal expansion[38]
278 and, for MEF and HFF cell lines, we utilized barrier bypass-clonal expansions prior to bulk whole-
279 genome sequencing. Recently, single-molecule duplex sequencing approaches have provided an
280 alternative high-fidelity protocol for directly measuring the mutagenic impact of genotoxic agents
281 without the need for clonal expansion, whilst improving the accuracy of NGS by more than 10,000-
282 fold and enabling sensitive detection of rare mutations, such as those induced by mutagens[39,53,54].
283 Importantly, duplex sequencing does not sequence a single cell or even a small number of cells,
284 rather, the method generally interrogates millions of double-stranded DNA coming from many
285 thousands of cells[55]. Thus, the mutational profile from duplex sequencing provides an average
286 somatic mutational profile across the complete population of exposed cells[39,53,54].
287
288 We used a commercial targeted duplex sequencing protocol for assessing mutagenesis without
289 clonal expansion[39] both to provide an orthogonal validation of the previous results and to account
290 for any potential artifacts due to clonal expansion in MEF and HFF cell lines. Specifically, we
291 detected somatic mutations using duplex sequencing data from 3 chronically irradiated and 3
292 unirradiated control HEKa cells (**Method**). Similar to irradiated HFFs and MEFs, chronically
293 exposed HEKa exhibited 1.3-fold increase of substitutions when compared to control cells (**Figure**
294 **6*a***; q-value: 0.02; Mann-Whitney test). Importantly, C>A transversions were 2.2-fold enriched in
295 chronically irradiate HEKa cells compared to control cells (q-values: 0.04; Mann-Whitney tests;

296 **Figure 6*b***). Moreover, a positive correlation between the number of C>A transversion and the
297 number of UV exposures was also evident in HEKa cells (**Figure 6*c***; Spearman's rank correlation:
298 0.88; p-value*:* 0.021). Consistent with prior results, no changes were observed for small insertions
299 or deletions between irradiated and control HEKa cells (**Figure 6*d***).
300
301 **Mutational Signatures Engraved by Irradiating with a UV-nail Polish Dryer**
302 Previously, we have shown that different endogenous and exogenous mutational processes engrave
303 characteristic patterns of somatic mutations, termed, mutational signatures[56-58]. To evaluate the
304 mutational signatures engraved by irradiation with a UV-nail polish dryer, we performed separate
305 analysis of mutational signatures for MEFs, HFFs, and HEKa data. To explain the SBS patterns
306 of mutations observed in the irradiated cells, any known COSMIC signature[59] that improved the
307 reconstruction above the background models was allowed. For the analyses of MEF data, in
308 addition to known COSMIC signatures, we also allowed mouses specific mutational signatures
309 previously observed either *in vitro*[52] or *in vivo*[60] murine models (**Supplementary Figure 7*a*)**.
310
311 Our analyses revealed that only COSMIC signatures SBS18 and SBS36 (SBS18/36), both
312 previously attributed to reactive oxygen species[61,62], were found to be operative in all irradiated
313 MEF and HFF cells. It should be noted that ROS signatures SBS18 and SBS36 have cosine
314 similarity of 0.914 (**Figure 7*a***), which, in many cases, makes them hard to distinguish from one
315 another and these signatures are commonly reported together as SBS18/36[35,63,64]. Our analyses
316 revealed that SBS18/36 were the only signatures enriched in irradiated HFF and MEF samples
317 when compared to controls (**Figure 7*b-c***; q-values<0.05; Mann-Whitney tests). No other
318 mutational signature found in these samples was elevated in irradiated samples when compared to

319 control samples (**Supplementary Figure** 7***b&d***). Moreover, the identified sets of operative
320 mutational signatures allowed accurately reconstructing the mutational patterns in both MEFs and
321 HFFs (**Supplementary Figure** 7***c&e***). The statistically significant increase of single base
322 substitutions between unirradiated and chronically irradiated cell lines that was attributed to the
323 ROS-associated signatures SBS18/36 was 0.70 and 0.14 mutations per megabase for MEF and
324 HFF, respectively (**Supplementary Figure 7**). This corresponds to an additional 2,000 and 400
325 ROS-associated somatic mutations engraved in the genome of a chronically irradiated MEF and
326 HFF cell, respectively.
327
328 Observing signatures SBS18/36, which are almost exclusively characterized by C>A substitutions
329 (**Figure 7*a***), in irradiated clones confirms that radiation emitted by a UV-nail polish dryer not only
330 oxidizes DNA but also results in permanently engraved patterns of C>A somatic mutations on the
331 genomes of irradiated cells. Similarly, an almost 3-fold enrichment of signatures SBS18/36 (p-
332 value < 0.0001; Fisher's exact test) was observed in keratinocytes irradiated with a UV-nail polish
333 dryer when compared to controls. Specifically, 65% of the mutations in UV-irradiated HEKa cells
334 were attributed to SBS18/36 (**Figure 7*d-e***). In contrast, in unirradiated control samples, SBS18/36
335 accounted for 23% of mutations (**Figure 7*d-e***).
336
337 Re-examination of the recently published set of 144 whole-genome sequenced skin cancers from
338 the Pan-Cancer Analysis of Whole Genomes (PCAWG) project[65] revealed a positive correlation
339 between C>A and C>T mutations (Pearson's correlation: 0.87; p-value < 2.2×10^{-16}; **Figure 7*f***).
340 Moreover, an average skin cancer appears to harbor approximately 2,500 C>A substitutions (95%
341 CI: 2,015 – 2,868) in their genome with approximately 80% of their pattern attributed to signatures

342 SBS18/36. However, these C>A substitutions account for only 2.3% of the mutations observed in
343 the 144 melanomas; 85% of mutations in these melanomas are generated by signature 7 –
344 mutational signature attributed to cyclobutane-pyrimidine dimers and 6-4 photoproducts from
345 ultraviolet light[65]. Importantly, 20 of the 169 substitutions (11.83%) identified as driver
346 mutations[65] in these samples can be attributed to signatures SBS18/36. This indicates that, while
347 signatures SBS18/36 generate low numbers of mutations in skin cancer, they play an important
348 role in generating somatic mutations that contribute towards tumor development and cancer
349 evolution.

350 **DISCUSSION**

351 In this report, we employed well-controlled experimental models for UV irradiation using a UV-
352 nail polish dryer and evaluated the DNA damage and mutagenic changes engraved on the genomes
353 of mammalian cells (**Figure 1**). The utilized *in vitro* clonal expansion models, MEFs and HFFs,
354 manifest the specific features required for mimicking human carcinogenesis and for recapitulating
355 the activity of characteristic mutational processes[38]. Importantly, the MEF model has proven to be
356 an invaluable *in vitro* model system for emulating human mutational signatures of various
357 exogenous and endogenous mutagens, including UVB and UVC radiation, known tobacco
358 carcinogens (*e.g.*, benzo[*a*]pyrene), aristolochic acid, and activation-induced cytidine deaminase
359 (AID)[66-70]. Both MEFs and HFFs underwent clonal expansion after a barrier bypass step
360 (senescence for MEFs and single-cell bottleneck for HFFs) leading to the formation of exposure-
361 derived clones, which were grown for the same number of doubling populations (**Supplementary**
362 **Figure 1**). Nevertheless, in some cases, these models may exhibit high background mutations due
363 to genomic instability occurring during clonal expansion process. As an orthogonal approach, we
364 also utilized HEKa primary cells, which cannot go through clonal expansion in culture.
365 Cytotoxicity and genotoxicity were observed in all irradiated cells; importantly, we observed an
366 elevation of ROS in irradiated cells leading to increased levels of 8-oxo-dG, which was confirmed
367 by multiple *in vitro* assays (**Figure 3**). Moreover, a potential mitochondrial dysfunction was
368 observed upon UVA radiation (**Figure 4** and **Supplementary Figure 4**). Genomic profiling
369 revealed higher levels of somatic mutations in irradiated cells with C>A mutations being highly
370 elevated in exposed samples (**Figures 5** and **6**). Consistent with the increase of ROS, COSMIC
371 signatures SBS18/36, two mutational signatures previously attributed to reactive oxygen

372 species[61,62], were engraved on the genomes of irradiated samples and enriched in irradiated
373 samples when compared to controls (**Figure 7**).
374
375 Broadband UVA (315-400nm) has been extensively studied in the context of tanning devices and
376 classified as carcinogen by the International Agency for Research on Cancer[13]. Broadband UVA
377 (315-400nm) penetrates deep in the skin, reaching the papillary dermis layer with longer-
378 wavelength UVA even reaching the deep dermis[71] and the stem cell compartments of the skin[72].
379 Prior experimental studies with broadband UVA have shown that it causes an accumulation of 8-
380 oxo-dG[20-24], generates C>A mutations in single-gene assays[25-28], and even induces tumors in
381 mice[73]. Indeed, prior studies have shown that UVA can generate low level of C>T somatic
382 mutations consistent with pyrimidine-pyrimidine photodimers[74]. Intriguingly, in this study, we
383 demonstrate that UVA with wavelengths between 365 and 395nm, which is generally considered
384 to be safe and is commonly used in a plethora of consumer products, causes DNA oxidative
385 damage leading to C>A mutations; no evidence was found that radiation generated by the UV-nail
386 polish machine generates any pyrimidine-pyrimidine photodimers (**Supplementary Figure 2**).
387 Importantly, the longer-wavelength of UVA emitted by a nail-polish dryer (365-395nm) will reach
388 all layers of the epidermis and it will penetrate towards the deeper layers of the dermis, potentially,
389 even affecting some skin stem cells. As keratinocytes are present in all layers of the epidermis and
390 melanocytes are found in the basal layer of epidermis, exposure to UVA from a nail-polish dryer
391 may irradiate these cells in a physiologically normal human skin.
392
393 Our findings are also consistent with prior cancer epidemiological observations. In principle, males
394 have significantly higher risk than females to develop melanoma[75,76]. Surprisingly, this trend is

395 reversed when one examines cancer risk in melanomas of the hand in younger women.
396 Specifically, young females (ages 15 to 39) have approximately 2-fold higher risk for developing
397 melanoma of the upper extremities compared to young males[77]. This higher risk is possibly due to
398 lifestyle choices, one of which may be radiation from consumer products such as UV-nail polish
399 dryers[77]. It should be noted that exposure to UV-light from the sun cannot reasonably explain the
400 higher risk in young females as there is no observed differences in melanoma risk between young
401 males and females for other parts of the body commonly exposed to the sunlight, *viz.*, face, head,
402 and neck[76,77].
403
404 While this report demonstrates that radiation from UV-nail polish dryers is cytotoxic, genotoxic,
405 and mutagenic, it does not provide direct evidence for increased cancer risk in human beings. Prior
406 studies have shown that an increase in mutagenesis will likely lead to an increase in cancer risk[78-
407 80]. Further, several anecdotal cases have demonstrated that cancers of the hand are likely due to
408 radiation from UV-nail polish dryers[32,34]. Taken together, our experimental results and the prior
409 evidence strongly suggest that radiation emitted by UV-nail polish dryers may cause cancers of
410 the hand and that UV-nail polish dryers, similar to tanning beds[81], may increase the risk of early-
411 onset skin cancer[82]. Nevertheless, future large-scale epidemiological studies are warranted to
412 accurately quantify the risk for skin cancer of the hand in people regularly using UV-nail polish
413 dryers. It is likely that such studies will take at least a decade to complete and to subsequently
414 inform the general public. In the meantime, this report aims to raise awareness of the likely cancer-
415 causing role of artificial UV lamps and caution people who regularly use UV-nail polish dryers.

416 **METHODS**

417 **UV-nail polish machine characteristics**

418 A 54-Watt UV nail drying machine was purchased (model: MelodySusie), harboring 6 bulbs that
419 emit UV photons for curing gel nail polish. Based on the manufacturer's specifications, the UV
420 nail drying machine emits ultraviolet A light in wavelengths between 365 and 395nm. The UV
421 power density was evaluated using a UV513AB Digital UVA/UVB Meter that can measure UV
422 radiation between 280 and 400 nm. The machine stabilizes at ~7.5 mW/cm^2, within minutes
423 (**Supplementary Figure 8*a-b*),** putting it on the lower end of the power density spectrum
424 calculated for commonly used UV-nail machines[31] (median of 10.6 mW/cm^2). In this study, in
425 most cases, we performed a 20-minute UV exposure session which is equivalent to a total amount
426 of energy delivered per unit area of 9 J/cm^2: *7.5 mW/cm^2 * 20 minutes = 7.5 mJ/(sec*cm^2) * 1200*
427 *sec = 9000 mJ/cm^2 = 9 J/cm^2.*

428

429 **Cell culture, irradiation, and immortalization of mouse embryonic fibroblasts (MEFs)**

430 Primary mouse embryonic fibroblasts (MEFs) were purchased from Lonza (M-FB-481). They
431 were expanded in Advanced DMEM supplemented with 15% fetal bovine serum, 1%
432 penicillin/streptomycin, 1% sodium pyruvate and 1% glutamine, and incubated in 20% O_2 and 5%
433 CO_2. At passage 2, the primary cells were seeded in six-well plates for 24 hours, until adherence,
434 then exposed for 20 minutes to the UV-nail machine in pre-warmed sterile PBS. Control cells were
435 kept in PBS for 20 minutes. Cells were irradiated with a UV nail polish dryer, acutely (*i.e.*, twice
436 a day, with 60 minutes break between each of the 2 sessions) as well as chronically (*i.e.*, once
437 every day for up to 3 consecutive days). At the end of every irradiation, the cells were washed, and
438 complete pre-warmed medium was replenished. Exposed and control primary cells were cultivated

439 until bypassed a barrier step through senescence. Upon barrier bypass, the cells reached clonal
440 expansion allowing the isolation of *bona fide* cell clones (**Supplementary Figure 1*a*)**. In all cases,
441 irradiated and control MEF cells were grown for ~28 doubling populations prior to bulk whole-
442 genome sequencing. Fifteen clonally expanded populations were successfully isolated and
443 subjected to bulk whole-genome sequencing, including: 5 replicates acute exposure, 5 replicates
444 of chronic exposure, and 5 replicates for unirradiated control cells. MEFs were authenticated by
445 PCR of the short tandem repeats (STR) to confirm the correct species and that they are
446 contamination-free. All cell cultures were routinely tested for the absence of mycoplasma.
447
448 **Cell culture, irradiation, and immortalization of human foreskin fibroblasts (HFFs)**
449 Primary human cells derived from human foreskin fibroblasts (HFFs) were provided to us by Dr.
450 John Murray (Indiana University Bloomington). Early passage cells were expanded in Advanced
451 DMEM supplemented with 10% fetal bovine serum and 1% glutamine in 5% CO_2 incubator.
452 Irradiation with a UV-nail polish dryer followed the same protocol as the one for MEFs (**Figure**
453 **1*a*)**. Similarly, control HFF cells were kept in PBS for 20 minutes during all irradiations. Clonal
454 expansion was carried out using serial dilutions procedure in 96-well plates, assuming 30%
455 probability of a single-cell clone formation per well (**Supplementary Figure 1*b*)**. Wells were
456 washed weekly, until clones reached confluency and were transferred progressively to T-75 flasks.
457 In all cases, irradiated and control HFF cells were grown for ~35 rounds of cell division. Fifteen
458 clonally expanded populations were successfully isolated and subjected to bulk whole-genome
459 sequencing, including: 5 replicates acute exposure, 5 replicates of chronic exposure, and 5
460 replicates for unirradiated control cells. HFFs were authenticated by PCR of the short tandem

461 repeats (STR) to confirm the correct species and that they are contamination-free. All cell cultures
462 were routinely tested for the absence of mycoplasma.
463
464 **Cell culture and irradiation of adult human epidermal keratinocytes (HEKa)**
465 Primary human keratinocytes, derived from normal adult human epidermal keratinocytes (HEKa),
466 were purchased from ATCC (PCS-200-011; Lot number: 70033063). Early passage cells were
467 expanded in Dermal Cell Basal Medium (PCS-200-030) supplemented with Keratinocyte Growth
468 Kit (PCS-200-040) and antibiotics (Penicillin: 10 Units/mL, Streptomycin: 10 μg/mL,
469 Amphotericin B: 25 ng/mL) in 5% CO_2 incubator. At passage 2, the primary cells were seeded at
470 a density of 2.5 x 10^3 cells/cm^2 in 10-cm dishes for 24 hours. Subsequently, cells were only
471 chronically irradiated with a UV-nail polish dryer following the same protocol as the for MEFs
472 and HFFs (**Figure 1*b***). Similarly, control HEKa cells were kept in PBS for 20 minutes during all
473 irradiations. In all cases, irradiated and control HEKa cells were grown for exactly 14 days,
474 corresponding to approximately 8 rounds of cell division, which allows sufficient time for DNA
475 adduct/damage to be fixed as somatic mutation(s) but not enough time to result in a clonal
476 expansion[39]. Unexposed cells were grown for the same duration as irradiated cells. Six cell
477 populations were successfully isolated and subjected to subjected to duplex sequencing, including:
478 3 replicates for chronic exposure and 3 replicates for unirradiated control cells. HEKa cells were
479 authenticated by PCR of the short tandem repeats (STR) to confirm the correct species and that
480 they are contamination-free. All cell cultures were routinely tested for the absence of mycoplasma.
481

482 **Cell viability and cytotoxicity assays**

483 Primary cells were seeded in 24-well plates and exposed to the UV drying device as indicated.
484 Cell viability was measured 48 hours after treatment cessation using the Cell-Counting Kit 8
485 (CCK-8) from Dojindo. Plates were incubated for 3 hours at 37°C and absorbance was measured
486 at 450 nm using the Infinite 200 Tecan *i*-control plate reader machine. The CCK-8 assay was
487 performed in at least 4 replicates for each experimental condition. Trypan Blue exclusion assay
488 was also performed for assessing cell viability upon exposure, validating the choice for selecting
489 the irradiation condition that causes around 50% cell death (**Supplementary Figure 8*c*)**.

490

491 **Assessment of genotoxicity using γH2Ax immunofluorescence**

492 Immunofluorescence staining was carried out using a monoclonal antibody specific for Ser139-
493 phosphorylated H2Ax (γH2Ax) (9718, Cell Signaling Technology). Briefly, primary cells were
494 seeded on coverslips in 24-well plates and, the following day, irradiated in triplicates as previously
495 described. Four hours after treatment cessation, the cells were fixed with 4% formaldehyde at room
496 temperature for 15 minutes, followed by blocking in 5% normal goat serum (5425, Life
497 Technologies) for 60 minutes. Subsequently, the cells were incubated with γH2Ax-antibody (1:400
498 in 1% BSA) at 4°C, overnight. A fluorochrome-conjugated anti-rabbit secondary antibody (4412,
499 Cell Signaling Technology), diluted to 1:1000, was then incubated for 1 hour at room temperature.
500 ß-actin staining was followed using phalloidin (8953, Cell Signaling Technology) incubated for
501 15 minutes at room temperature. Coverslips were mounted in ProLong Gold Antifade Reagent
502 with DAPI (8961, Cell Signaling Technology), overnight. Immunofluorescence images were
503 captured using a Confocal Laser Scanning Biological Microscope Olympus FV1000 Fluoview.
504 Quantification of γH2Ax fluorescent cells was computed using Fiji software (version 2.3.0).

505

506 **Investigation of photoproducts using CPD and 6-4PP immunofluorescence**

507 Immunofluorescence staining was carried out using anti-cyclobutane pyrimidine dimers (CPDs)
508 monoclonal antibodies (clone KTM53, Kamiya Biomedical) and anti-6-4 photoproducts
509 monoclonal antibodies (Clone 64M-2, Cosmo Bio). Briefly, primary cells were seeded on
510 coverslips in 24-well plates and, the following day, irradiated in triplicates as previously described.
511 Subsequently, the cells were washed with ice-cold CSK buffer, containing 100mM NaCl, 300mM
512 Glucose, 10mM PIPES, 3mM MgCl2 and 0.5% Triton, then fixed with 4% formaldehyde at room
513 temperature (RT) for 15 minutes, followed by permeabilization using 0.5% Triton for 5 minutes
514 on ice. DNase I treatment was performed to denaturalize the genomic DNA in the cells using 20U
515 DNase I for 40s per coverslip (NEB; DNase I (RNase-free), M0303S). For blocking, we used 1%
516 BSA (A3059, Sigma) and 5% normal goat serum (5425, Life Technologies) for 60 minutes.
517 Afterwards, the cells were incubated with the monoclonal antibodies (1:50 in 1% BSA) at 4°C,
518 overnight. A fluorochrome-conjugated anti-mouse Alexa Fluor 594 secondary antibody (8890S,
519 Cell Signaling Technology), diluted to 1:1000, was then incubated for 1 hour at room temperature.
520 Coverslips were mounted in ProLong Gold Antifade Reagent with DAPI (8961, Cell Signaling
521 Technology), overnight. Immunofluorescence images were captured using Nikon A1R-STORM
522 Super Resolution Microscope and processed on Fiji software (version 2.3.0).

523

524 **Quantification of reactive oxygen species via CellROX**

525 Oxidative stress induces the production of reactive oxygen species (ROS) and reactive nitrogen
526 species (RNS) in cells. We employed the CellROX™ Green Reagent for detection of oxidative
527 stress (ThermoFisher Scientific; catalog number: C10444), immediately after irradiation. MEF,

528 HFF, and HEKa primary cells were seeded on Mattek 35-mm dishes from (P35G-1.5-14-C)
529 appropriate for high quality live cell imaging. CellROX green was added in pre-warmed complete
530 media to a final concentration of 5µM and incubated for 30 minutes at 37 ºC. CellROX solution
531 was washed carefully 3 times with pre-warmed PBS and normal media was replenished. Live cell
532 imaging was conducted using Nikon A1R-STORM Super Resolution Microscope and processed
533 on Fiji software (version 2.3.0). To ensure CellROX selectivity towards ROS components, cells
534 were challenged with 2mM N-acetyl-L-cysteine (NAC) for 1 hour prior to UVA exposure. NAC
535 is a known ROS scavenger. After CellROX addition, live cell images were used for quantification
536 of CellROX foci number, with and without NAC pre-treatment, using General Analysis pipeline
537 on Nikon WorkStation 5317.
538
539 **Quantification of reactive oxygen species via OxiSelect**
540 Additionally, we also utilized the OxiSelect™ *In Vitro* ROS/RNS Assay Kit (Green Fluorescence),
541 from Cell Biolabs, to evaluate the level of oxidative damage induced after irradiation, intra- and
542 extra-cellularly, immediately after exposure as well as 20 minutes and 1 day after irradiation.
543 Primary MEFs and HFFs were irradiated in triplicates in a 6-well plate, twice a day (acute
544 exposure) and once every day for 3 consecutive days (chronic exposure). PBS solutions were
545 collected immediately after the last UV treatments. After every treatment, the cells were washed
546 with pre-warmed PBS and complete media was replenished for the accounted waiting timepoints.
547 Thereafter, media solutions were collected 20 minutes and 24 hours after treatment cessation.
548 These solutions were used to assess extracellular ROS signals. Cytosolic ROS production was
549 evaluated after trypsinization of the cells, lysis of cellular membrane with 0.5% TritonX-100 and
550 centrifugation for 5 minutes at 14,000 x g. Samples were loaded into a 96 black well plate, together

551 with varying concentrations of hydrogen peroxide for generating the standard curve, and
552 fluorescence signals were recorded using the Infinite 200 Tecan *i*-control plate reader machine at
553 480 nm excitation / 530 nm emission.
554
555 **Quantification of 8-hydroxy-2'-deoxyguanosine via ELISA**
556 We quantified 8-hydroxy-2'-deoxyguanosine (8-oxo-dG) for oxidative DNA damage in DNA
557 samples using the EpiQuik™ 8-OHdG DNA Damage Quantification Direct Kit (Colorimetric)
558 from Epigentek following manufacturer instructions. Briefly, primary MEF, HFF, and HEKa
559 primary cells were seeded on 10-cm dishes overnight. Three positive control exposures were
560 employed, after concentration optimization, namely 400μM H_2O_2 for 1 hour, 20J/m^2 UVC, and
561 4mM $KBrO_3$ for 1 hour. Following irradiation with nail polish dryer, cells were collected at the
562 selected timepoints (immediately, 4 hours, and 24 hours after irradiation) and subjected to genomic
563 DNA extraction. Following Qubit DNA quantification, 300ng of DNA was loaded into strip wells
564 that are specifically treated to have a high DNA affinity. 8-oxo-dG was detected using capture and
565 detection antibodies. The detected signal is enhanced, and the readout was measured at 450 nm
566 absorbance using the Infinite 200 Tecan *i*-control plate reader machine.
567
568 **Evaluation of mitochondrial ROS production and membrane potential**
569 Image-iT™ TMRM Reagent, and MitoSOX™ Red Mitochondrial Superoxide Indicator
570 (ThermoFisher Scientific; catalog number: I34361 and M36008, respectively), are two dyes that
571 target mitochondria in live cells, the former localizing active mitochondria with normal
572 mitochondria membrane potential, and the latter with affinity to ROS production. MitoTracker™
573 Green FM (ThermoFisher Scientific, catalog number: M7514) was utilized to localize

574 mitochondria regardless of mitochondrial membrane potential. Briefly, primary cells were seeded
575 on Mattek 35-mm dishes (P35G-1.5-14-C) overnight and incubated for 30 minutes in pre-warmed
576 live imaging staining solution (ThermoFisher Scientific, catalog number: A14291DJ) containing
577 100µM MitoTracker reagent. TMRM dye was added in pre-warmed Live Imagining Solution to a
578 final concentration of 100nM and incubated for 30 minutes at 37 ºC. MitoSOX solution was
579 prepared in pre-warmed Live Imagining Solution to a final concentration of 200nM and incubated
580 for 10 minutes at 37 ºC. All solutions were washed carefully 3 times with pre-warmed PBS and
581 normal media was replenished. Live cell imaging was conducted using Nikon A1R-STORM Super
582 Resolution Microscope and processed on Fiji software (version 2.3.0). Fluorescence data
583 quantification was carried out using General Analysis pipeline on Nikon WorkStation 5317.
584
585 **DNA extraction and bulk whole-genome sequencing**
586 Genomic DNA from MEF and HFF primary cells and immortalized clones were extracted using
587 Qiagen DNeasy Blood & Tissue kit, following the manufacturer instructions. Quality and quantity
588 of DNA were checked using NanoDrop and Qubit instruments. Around 2ug of DNA was thereby
589 extracted per each sample. High-quality DNA for 32 samples were sent to Novogene for whole-
590 genome library preparation and whole-genome sequencing at 30x coverage using paired-end 150
591 base-pair run mode with Illumina's HiSeq-XTen. The 32 samples included: *(i)* one primary HFF
592 and one primary MEF used as normal samples in the mutation calling; *(ii)* 5 HFF and 5 MEF
593 immortalized clones after acute irradiation; *(iii)* 5 HFF and 5 MEF immortalized clones after
594 chronic irradiation; and *(iv)* 5 HFF and 5 MEF unirradiated immortalized control clones.
595

596 **Identification of somatic mutations from whole-genome bulk sequencing**

597 FASTQ files were subjected to BWA-MEM alignment using GRCm38 and GRCh38 as reference
598 genomes for MEF and HFF, respectively. Our methodology for identification of somatic mutations
599 from bulk sequencing data follows established approaches from large genomics consortia[83,84].
600 Briefly, ensemble variant calling of somatic mutations was performed using three independent
601 variant callers Mutect2[85], VarScan2[86], Strelka2[87], and MuSe[88]. Any mutation identified by at least
602 two out of the four variant callers was considered a *bona fide* mutation. *Bona fide* mutations were
603 subsequently filtered to remove any residual SNPs based on dbSNP annotation by variant effect
604 predictor[89]. Further, any mutations shared between two or more samples and clustered mutations
605 were removed as these reflect either residual germline mutations or mutations under positive
606 selection (**Supplementary Figure 5**). Overall, a total of 118,429 unique somatic mutations were
607 detected across all sequenced samples prior to filtering. Consistent with prior datasets[83,84], the
608 germline filtering removed 18.7% of these mutations with another 5.2% removed by the clustered
609 filter. The remaining set of somatic mutations were used in the subsequent analyses and the
610 evaluation for mutational signatures. Somatic copy-number changes were detected using
611 FACETS[90] with default parameters using the wrapper script cnv_facets v0.16.0.

612

613 **DNA extraction and duplex sequencing**

614 Genomic DNA from HEKa cells were extracted using Qiagen DNeasy Blood & Tissue kit,
615 following manufacturer instructions, with one exception during the initial proteinaseK digestion
616 for which the samples were incubated at 37℃ rather than 54℃ for 1 hour, and DNA yield was
617 eluted in IDTE buffer (10mM Tris HCl pH 8.0 + 0.1mM EDTA). Quality and quantity of DNA
618 were checked using NanoDrop and Qubit instruments. High-quality DNA for 7 samples were sent

619 to TwinStrand Biosciences for targeted library preparation, targeted duplex sequencing, and data
620 analysis. The seven samples included: *(i)* one primary HEKa sample used in the mutation calling;
621 *(ii)* 3 HEKa samples after chronic irradiation; and *(iii)* 3 HEKa unirradiated immortalized control
622 clones. Briefly, duplex library preparation was performed using a human mutagenesis panel (~50
623 kb distributed across the whole genome in regions not predicted to be under positive or negative
624 selection) on DNA input sufficient to generate between 500 million to 1 billion informative Duplex
625 base pairs per sample. Each sample was prepared in two batches: one with the standard
626 mutagenesis assay and one with a prototype rapid workflow version of the assay. All libraries were
627 sequenced on an Illumina NovaSeq 6000.
628
629 **Identification of somatic mutations from duplex sequencing**
630 All raw NovaSeq sequencing FASTQ data was processed through the TwinStrand cloud-based
631 human mutagenesis pipeline to generate error-corrected BAM files and variant call files for each
632 sample. Duplex sequencing yielded an average of ~239 million raw reads per sample, an average
633 of ~982 million duplex bases per sample, and an average of 15.204x on target duplex depth. No
634 interspecies or intra-sample contamination found. Hybrid selection efficacy was approximately
635 99.81%. Mutagenesis analysis was carried out using the *Min* assumption for mutant frequency
636 calculation as standardly done[39]. This method counts each variant only once, regardless of the
637 number of reads that contain the non-reference allele. As previously done, the variant allelic
638 frequency of each mutations was calculated by dividing the number of unique variants to the total
639 number of duplex bases[39]. The set of somatic mutations with variant allelic frequency ≤ 1% were
640 used in the subsequent analyses and the evaluation for mutational signatures.
641

642 **Analysis of mutational signatures and additional examinations**

643 Analysis of mutational signatures was performed using our previously derived set of reference
644 mutational signatures[59] as well as our previously established methodology with the SigProfiler
645 suite of tools used for summarization, simulation, visualization, and assignment of mutational
646 signatures[91-94]. Variant allele frequencies (VAF) were calculated using integrative genomics
647 viewer[95]. R version 3.6.1 was used to plot data (*i.e.,* ggplot2, easyGgplot2, ComplexHeatmap[96],
648 and circlize[97] packages), to compute p-values (ggpubr package), to perform correlation analyses
649 (corrr package), and to compute the cosine similarity (lsa[98] package).

650

651 **Statistics and Reproducibility**

652 Unless otherwise annotated, all statistical comparisons were performed using Mann-Whitney U
653 two-sided tests. All data generated in this study were collected from at least triplicates, unless
654 otherwise stated. Each experiment was performed at least three times independently with
655 reproducible results. All immunofluorescence images were collected from triplicates and each
656 assay was performed three times. No statistical method was used to predetermine sample size. No
657 data were excluded from the performed analyses. Our experiments were not randomized. The
658 investigators were not blinded to allocations during experiments and outcome assessment.

659

660 **DATA AVAILABILITY**

661 All whole-genome and duplex sequencing data have been deposited to Sequence Read Archive
662 (SRA) and can be downloaded using accession number: PRJNA667106. All data and metadata
663 for the previously generated whole-genome sequenced skin cancers were obtained from the
664 official PCAWG release (https://dcc.icgc.org/releases/PCAWG). Where appropriate, source data

665 are provided for the figures in the paper. For mouse samples, we aligned FASTQ file to the
666 GRCm38 reference genome. For human samples, we aligned FASTQ files to the GRCh38
667 reference genome. We employed the dbSNP142 for germline mutations filtration in mouse
668 samples, and dbSNP155 for human samples.
669
670 **CODE AVAILABILITY**
671 Somatic mutations in whole-genome sequencing data were identified using our ensemble variant
672 calling pipeline, which is freely available under the permissive 2-clause BSD license
673 at: https://github.com/AlexandrovLab/EnsembleVariantCallingPipeline. All other computational
674 tools utilized in this publication have been previously published and can be access through their
675 respective publications.
676

677 **REFERENCES**

678 1 Khan, A. Q., Travers, J. B. & Kemp, M. G. Roles of UVA radiation and DNA damage
679 responses in melanoma pathogenesis. *Environ Mol Mutagen* **59**, 438-460,
680 doi:10.1002/em.22176 (2018).
681 2 Pfeifer, G. P. Mechanisms of UV-induced mutations and skin cancer. *Genome Instab Dis*
682 **1**, 99-113, doi:10.1007/s42764-020-00009-8 (2020).
683 3 You, Y. H., Szabó, P. E. & Pfeifer, G. P. Cyclobutane pyrimidine dimers form
684 preferentially at the major p53 mutational hotspot in UVB-induced mouse skin tumors.
685 *Carcinogenesis* **21**, 2113-2117, doi:10.1093/carcin/21.11.2113 (2000).
686 4 Pfeifer, G. P. Formation and processing of UV photoproducts: effects of DNA sequence
687 and chromatin environment. *Photochem Photobiol* **65**, 270-283, doi:10.1111/j.1751-
688 1097.1997.tb08560.x (1997).
689 5 Cadet, J. *et al.* Effects of UV and visible radiation on DNA-final base damage. *Biol Chem*
690 **378**, 1275-1286 (1997).
691 6 Cadet, J., Douki, T. & Ravanat, J. L. Oxidatively generated damage to cellular DNA by
692 UVB and UVA radiation. *Photochem Photobiol* **91**, 140-155, doi:10.1111/php.12368
693 (2015).
694 7 Zhang, X. *et al.* Induction of 8-oxo-7,8-dihydro-2'-deoxyguanosine by ultraviolet radiation
695 in calf thymus DNA and HeLa cells. *Photochem Photobiol* **65**, 119-124,
696 doi:10.1111/j.1751-1097.1997.tb01886.x (1997).
697 8 Besaratinia, A. *et al.* DNA lesions induced by UV A1 and B radiation in human cells:
698 comparative analyses in the overall genome and in the p53 tumor suppressor gene. *Proc*
699 *Natl Acad Sci U S A* **102**, 10058-10063, doi:10.1073/pnas.0502311102 (2005).
700 9 Schuch, A. P., Moreno, N. C., Schuch, N. J., Menck, C. F. M. & Garcia, C. C. M. Sunlight
701 damage to cellular DNA: Focus on oxidatively generated lesions. *Free Radic Biol Med*
702 **107**, 110-124, doi:10.1016/j.freeradbiomed.2017.01.029 (2017).
703 10 Brem, R., Li, F. & Karran, P. Reactive oxygen species generated by thiopurine/UVA cause
704 irreparable transcription-blocking DNA lesions. *Nucleic Acids Res* **37**, 1951-1961,
705 doi:10.1093/nar/gkp070 (2009).
706 11 Douki, T. & Sage, E. Dewar valence isomers, the third type of environmentally relevant
707 DNA photoproducts induced by solar radiation. *Photochem Photobiol Sci* **15**, 24-30,
708 doi:10.1039/c5pp00382b (2016).
709 12 Rochette, P. J. *et al.* UVA-induced cyclobutane pyrimidine dimers form predominantly at
710 thymine-thymine dipyrimidines and correlate with the mutation spectrum in rodent cells.
711 *Nucleic Acids Res* **31**, 2786-2794, doi:10.1093/nar/gkg402 (2003).
712 13 El Ghissassi, F. *et al.* A review of human carcinogens--part D: radiation. *Lancet Oncol* **10**,
713 751-752, doi:10.1016/s1470-2045(09)70213-x (2009).
714 14 Sample, A. & He, Y. Y. Mechanisms and prevention of UV-induced melanoma.
715 *Photodermatol Photoimmunol Photomed* **34**, 13-24, doi:10.1111/phpp.12329 (2018).
716 15 cancer, I. A. f. R. o. C. W. G. o. a. u. U. l. a. s. The association of use of sunbeds with
717 cutaneous malignant melanoma and other skin cancers: A systematic review. *Int J Cancer*
718 **120**, 1116-1122, doi:10.1002/ijc.22453 (2007).
719 16 van Weelden, H., de Gruijl, F. R., van der Putte, S. C., Toonstra, J. & van der Leun, J. C.
720 The carcinogenic risks of modern tanning equipment: is UV-A safer than UV-B? *Arch*
721 *Dermatol Res* **280**, 300-307, doi:10.1007/bf00440604 (1988).

722 17 van Weelden, H., van der Putte, S. C., Toonstra, J. & van der Leun, J. C. UVA-induced
723 tumours in pigmented hairless mice and the carcinogenic risks of tanning with UVA. *Arch*
724 *Dermatol Res* **282**, 289-294, doi:10.1007/bf00375721 (1990).
725 18 Sterenborg, H. J. & van der Leun, J. C. Tumorigenesis by a long wavelength UV-A source.
726 *Photochem Photobiol* **51**, 325-330, doi:10.1111/j.1751-1097.1990.tb01718.x (1990).
727 19 Kelfkens, G., de Gruijl, F. R. & van der Leun, J. C. Tumorigenesis by short-wave
728 ultraviolet A: papillomas versus squamous cell carcinomas. *Carcinogenesis* **12**, 1377-
729 1382, doi:10.1093/carcin/12.8.1377 (1991).
730 20 Greinert, R. *et al.* UVA-induced DNA double-strand breaks result from the repair of
731 clustered oxidative DNA damages. *Nucleic Acids Res* **40**, 10263-10273,
732 doi:10.1093/nar/gks824 (2012).
733 21 Didier, C., Emonet-Piccardi, N., Béani, J. C., Cadet, J. & Richard, M. J. L-arginine
734 increases UVA cytotoxicity in irradiated human keratinocyte cell line: potential role of
735 nitric oxide. *FASEB J* **13**, 1817-1824, doi:10.1096/fasebj.13.13.1817 (1999).
736 22 Francis, A. J. & Giannelli, F. Cooperation between human cells sensitive to UVA
737 radiations: a clue to the mechanism of cellular hypersensitivity associated with different
738 clinical conditions. *Exp Cell Res* **195**, 47-52, doi:10.1016/0014-4827(91)90498-j (1991).
739 23 Eisenstark, A. Mutagenic and lethal effects of near-ultraviolet radiation (290-400 nm) on
740 bacteria and phage. *Environ Mol Mutagen* **10**, 317-337, doi:10.1002/em.2850100311
741 (1987).
742 24 Ridley, A. J., Whiteside, J. R., McMillan, T. J. & Allinson, S. L. Cellular and sub-cellular
743 responses to UVA in relation to carcinogenesis. *Int J Radiat Biol* **85**, 177-195,
744 doi:10.1080/09553000902740150 (2009).
745 25 Besaratinia, A., Bates, S. E., Synold, T. W. & Pfeifer, G. P. Similar mutagenicity of
746 photoactivated porphyrins and ultraviolet A radiation in mouse embryonic fibroblasts:
747 involvement of oxidative DNA lesions in mutagenesis. *Biochemistry* **43**, 15557-15566,
748 doi:10.1021/bi048717c (2004).
749 26 Besaratinia, A., Kim, S. I., Bates, S. E. & Pfeifer, G. P. Riboflavin activated by ultraviolet
750 A1 irradiation induces oxidative DNA damage-mediated mutations inhibited by vitamin C.
751 *Proc Natl Acad Sci U S A* **104**, 5953-5958, doi:10.1073/pnas.0610534104 (2007).
752 27 Kim, S. I., Pfeifer, G. P. & Besaratinia, A. Mutagenicity of ultraviolet A radiation in the
753 lacI transgene in Big Blue mouse embryonic fibroblasts. *Mutat Res* **617**, 71-78,
754 doi:10.1016/j.mrfmmm.2006.12.003 (2007).
755 28 Pfeifer, G. P., You, Y. H. & Besaratinia, A. Mutations induced by ultraviolet light. *Mutat*
756 *Res* **571**, 19-31, doi:10.1016/j.mrfmmm.2004.06.057 (2005).
757 29 Rieder, E. A. & Tosti, A. Cosmetically Induced Disorders of the Nail with Update on
758 Contemporary Nail Manicures. *J Clin Aesthet Dermatol* **9**, 39-44 (2016).
759 30 Bollard, S. M. *et al.* Skin cancer risk and the use of UV nail lamps. *Australas J Dermatol*
760 **59**, 348-349, doi:10.1111/ajd.12806 (2018).
761 31 Shipp, L. R., Warner, C. A., Rueggeberg, F. A. & Davis, L. S. Further investigation into
762 the risk of skin cancer associated with the use of UV nail lamps. *JAMA Dermatol* **150**, 775-
763 776, doi:10.1001/jamadermatol.2013.8740 (2014).
764 32 Ratycz, M. C., Lender, J. A. & Gottwald, L. D. Multiple Dorsal Hand Actinic Keratoses
765 and Squamous Cell Carcinomas: A Unique Presentation following Extensive UV Nail
766 Lamp Use. *Case Rep Dermatol* **11**, 286-291, doi:10.1159/000503273 (2019).

33 Ceballos, D. M. *et al.* Biological and environmental exposure monitoring of volatile organic compounds among nail technicians in the Greater Boston area. *Indoor Air* **29**, 539-550, doi:10.1111/ina.12564 (2019).
34 MacFarlane, D. F. & Alonso, C. A. Occurrence of nonmelanoma skin cancers on the hands after UV nail light exposure. *Arch Dermatol* **145**, 447-449, doi:10.1001/archdermatol.2008.622 (2009).
35 Levatić, J., Salvadores, M., Fuster-Tormo, F. & Supek, F. Mutational signatures are markers of drug sensitivity of cancer cells. *Nat Commun* **13**, 2926, doi:10.1038/s41467-022-30582-3 (2022).
36 Jin, S. G., Meng, Y., Johnson, J., Szabó, P. E. & Pfeifer, G. P. Concordance of hydrogen peroxide-induced 8-oxo-guanine patterns with two cancer mutation signatures of upper GI tract tumors. *Sci Adv* **8**, eabn3815, doi:10.1126/sciadv.abn3815 (2022).
37 Zou, X. *et al.* A systematic CRISPR screen defines mutational mechanisms underpinning signatures caused by replication errors and endogenous DNA damage. *Nat Cancer* **2**, 643-657, doi:10.1038/s43018-021-00200-0 (2021).
38 Zhivagui, M., Korenjak, M. & Zavadil, J. Modelling Mutation Spectra of Human Carcinogens Using Experimental Systems. *Basic Clin Pharmacol Toxicol* **121 Suppl 3**, 16-22, doi:10.1111/bcpt.12690 (2017).
39 Schmitt, M. W. *et al.* Detection of ultra-rare mutations by next-generation sequencing. *Proc Natl Acad Sci U S A* **109**, 14508-14513, doi:10.1073/pnas.1208715109 (2012).
40 Sharma, A., Singh, K. & Almasan, A. Histone H2AX phosphorylation: a marker for DNA damage. *Methods Mol Biol* **920**, 613-626, doi:10.1007/978-1-61779-998-3_40 (2012).
41 Budden, T. & Bowden, N. A. The role of altered nucleotide excision repair and UVB-induced DNA damage in melanomagenesis. *Int J Mol Sci* **14**, 1132-1151, doi:10.3390/ijms14011132 (2013).
42 Yang, Z. & Choi, H. Single-Cell, Time-Lapse Reactive Oxygen Species Detection in E. coli. *Curr Protoc Cell Biol* **80**, e60, doi:10.1002/cpcb.60 (2018).
43 Suzuki, T. & Kamiya, H. Mutations induced by 8-hydroxyguanine (8-oxo-7,8-dihydroguanine), a representative oxidized base, in mammalian cells. *Genes Environ* **39**, 2, doi:10.1186/s41021-016-0051-y (2017).
44 Douki, T. *et al.* Oxidation of guanine in cellular DNA by solar UV radiation: biological role. *Photochem Photobiol* **70**, 184-190 (1999).
45 KESTON, A. S. & BRANDT, R. THE FLUOROMETRIC ANALYSIS OF ULTRAMICRO QUANTITIES OF HYDROGEN PEROXIDE. *Anal Biochem* **11**, 1-5, doi:10.1016/0003-2697(65)90034-5 (1965).
46 Ezeriņa, D., Takano, Y., Hanaoka, K., Urano, Y. & Dick, T. P. N-Acetyl Cysteine Functions as a Fast-Acting Antioxidant by Triggering Intracellular H. *Cell Chem Biol* **25**, 447-459.e444, doi:10.1016/j.chembiol.2018.01.011 (2018).
47 BRANDT, R. & KESTON, A. S. SYNTHESIS OF DIACETYLDICHLOROFLUORESCIN: A STABLE REAGENT FOR FLUOROMETRIC ANALYSIS. *Anal Biochem* **11**, 6-9, doi:10.1016/0003-2697(65)90035-7 (1965).
48 Bass, D. A. *et al.* Flow cytometric studies of oxidative product formation by neutrophils: a graded response to membrane stimulation. *J Immunol* **130**, 1910-1917 (1983).
49 Murphy, M. P. How mitochondria produce reactive oxygen species. *Biochem J* **417**, 1-13, doi:10.1042/BJ20081386 (2009).

50 Brand, R. M. *et al.* Targeting Mitochondrial Oxidative Stress to Mitigate UV-Induced Skin Damage. *Front Pharmacol* **9**, 920, doi:10.3389/fphar.2018.00920 (2018).
51 Qian, W. *et al.* Chemoptogenetic damage to mitochondria causes rapid telomere dysfunction. *Proc Natl Acad Sci U S A* **116**, 18435-18444, doi:10.1073/pnas.1910574116 (2019).
52 Zhivagui, M. *et al.* Experimental and pan-cancer genome analyses reveal widespread contribution of acrylamide exposure to carcinogenesis in humans. *Genome Res* **29**, 521-531, doi:10.1101/gr.242453.118 (2019).
53 Salk, J. J., Schmitt, M. W. & Loeb, L. A. Enhancing the accuracy of next-generation sequencing for detecting rare and subclonal mutations. *Nat Rev Genet* **19**, 269-285, doi:10.1038/nrg.2017.117 (2018).
54 Salk, J. J. & Kennedy, S. R. Next-Generation Genotoxicology: Using Modern Sequencing Technologies to Assess Somatic Mutagenesis and Cancer Risk. *Environ Mol Mutagen* **61**, 135-151, doi:10.1002/em.22342 (2020).
55 Abbasi, A. & Alexandrov, L. B. Significance and limitations of the use of next-generation sequencing technologies for detecting mutational signatures. *DNA Repair (Amst)* **107**, 103200, doi:10.1016/j.dnarep.2021.103200 (2021).
56 Alexandrov, L. B. *et al.* Signatures of mutational processes in human cancer. *Nature* **500**, 415-421, doi:10.1038/nature12477 (2013).
57 Alexandrov, L. B. & Stratton, M. R. Mutational signatures: the patterns of somatic mutations hidden in cancer genomes. *Curr Opin Genet Dev* **24**, 52-60, doi:10.1016/j.gde.2013.11.014 (2014).
58 Alexandrov, L. B. & Zhivagui, M. in *Encyclopedia of Cancer (Third Edition)* 499-510 (2019).
59 Alexandrov, L. B., Nik-Zainal, S., Wedge, D. C., Campbell, P. J. & Stratton, M. R. Deciphering signatures of mutational processes operative in human cancer. *Cell Rep* **3**, 246-259, doi:10.1016/j.celrep.2012.12.008 (2013).
60 Riva, L. *et al.* The mutational signature profile of known and suspected human carcinogens in mice. *Nat Genet* **52**, 1189-1197, doi:10.1038/s41588-020-0692-4 (2020).
61 Pilati, C. *et al.* Mutational signature analysis identifies MUTYH deficiency in colorectal cancers and adrenocortical carcinomas. *J Pathol* **242**, 10-15, doi:10.1002/path.4880 (2017).
62 Viel, A. *et al.* A Specific Mutational Signature Associated with DNA 8-Oxoguanine Persistence in MUTYH-defective Colorectal Cancer. *EBioMedicine* **20**, 39-49, doi:10.1016/j.ebiom.2017.04.022 (2017).
63 Georgeson, P. *et al.* Identifying colorectal cancer caused by biallelic MUTYH pathogenic variants using tumor mutational signatures. *Nat Commun* **13**, 3254, doi:10.1038/s41467-022-30916-1 (2022).
64 Georgeson, P. *et al.* Evaluating the utility of tumour mutational signatures for identifying hereditary colorectal cancer and polyposis syndrome carriers. *Gut* **70**, 2138-2149, doi:10.1136/gutjnl-2019-320462 (2021).
65 Alexandrov, L. B. *et al.* The repertoire of mutational signatures in human cancer. *Nature* **578**, 94-101, doi:10.1038/s41586-020-1943-3 (2020).
66 Olivier, M. *et al.* Modelling mutational landscapes of human cancers in vitro. *Sci Rep* **4**, 4482, doi:10.1038/srep04482 (2014).

858 67 Nik-Zainal, S. *et al.* The genome as a record of environmental exposure. *Mutagenesis* **30**,
859 763-770, doi:10.1093/mutage/gev073 (2015).
860 68 Besaratinia, A. & Pfeifer, G. P. Applications of the human p53 knock-in (Hupki) mouse
861 model for human carcinogen testing. *FASEB J* **24**, 2612-2619, doi:10.1096/fj.10-157263
862 (2010).
863 69 Zavadil, J. & Rozen, S. G. Experimental Delineation of Mutational Signatures Is an
864 Essential Tool in Cancer Epidemiology and Prevention. *Chem Res Toxicol* **32**, 2153-2155,
865 doi:10.1021/acs.chemrestox.9b00339 (2019).
866 70 Phillips, D. H. Mutational spectra and mutational signatures: Insights into cancer aetiology
867 and mechanisms of DNA damage and repair. *DNA Repair (Amst)* **71**, 6-11,
868 doi:10.1016/j.dnarep.2018.08.003 (2018).
869 71 Battie, C. *et al.* New insights in photoaging, UVA induced damage and skin types. *Exp*
870 *Dermatol* **23 Suppl 1**, 7-12, doi:10.1111/exd.12388 (2014).
871 72 Agar, N. S. *et al.* The basal layer in human squamous tumors harbors more UVA than UVB
872 fingerprint mutations: a role for UVA in human skin carcinogenesis. *Proc Natl Acad Sci U*
873 *S A* **101**, 4954-4959, doi:10.1073/pnas.0401141101 (2004).
874 73 Trucco, L. D. *et al.* Ultraviolet radiation-induced DNA damage is prognostic for outcome
875 in melanoma. *Nat Med* **25**, 221-224, doi:10.1038/s41591-018-0265-6 (2019).
876 74 Moreno, N. C. *et al.* Whole-exome sequencing reveals the impact of UVA light
877 mutagenesis in xeroderma pigmentosum variant human cells. *Nucleic Acids Res* **48**, 1941-
878 1953, doi:10.1093/nar/gkz1182 (2020).
879 75 Feigelson, H. S. *et al.* Melanoma incidence, recurrence, and mortality in an integrated
880 healthcare system: A retrospective cohort study. *Cancer Med* **8**, 4508-4516,
881 doi:10.1002/cam4.2252 (2019).
882 76 Ferlay, J. *et al.* Estimating the global cancer incidence and mortality in 2018: GLOBOCAN
883 sources and methods. *Int J Cancer* **144**, 1941-1953, doi:10.1002/ijc.31937 (2019).
884 77 Weir, H. K. *et al.* Melanoma in adolescents and young adults (ages 15-39 years): United
885 States, 1999-2006. *J Am Acad Dermatol* **65**, S38-49, doi:10.1016/j.jaad.2011.04.038
886 (2011).
887 78 Tomasetti, C., Marchionni, L., Nowak, M. A., Parmigiani, G. & Vogelstein, B. Only three
888 driver gene mutations are required for the development of lung and colorectal cancers. *Proc*
889 *Natl Acad Sci U S A* **112**, 118-123, doi:10.1073/pnas.1421839112 (2015).
890 79 Tomasetti, C., Li, L. & Vogelstein, B. Stem cell divisions, somatic mutations, cancer
891 etiology, and cancer prevention. *Science* **355**, 1330-1334, doi:10.1126/science.aaf9011
892 (2017).
893 80 Balmain, A. The critical roles of somatic mutations and environmental tumor-promoting
894 agents in cancer risk. *Nat Genet* **52**, 1139-1143, doi:10.1038/s41588-020-00727-5 (2020).
895 81 Zhang, M. *et al.* Use of tanning beds and incidence of skin cancer. *J Clin Oncol* **30**, 1588-
896 1593, doi:10.1200/JCO.2011.39.3652 (2012).
897 82 O'Sullivan, N. A. & Tait, C. P. Tanning bed and nail lamp use and the risk of cutaneous
898 malignancy: a review of the literature. *Australas J Dermatol* **55**, 99-106,
899 doi:10.1111/ajd.12145 (2014).
900 83 Consortium, I. T. P.-C. A. o. W. G. Pan-cancer analysis of whole genomes. *Nature* **578**,
901 82-93, doi:10.1038/s41586-020-1969-6 (2020).

84 Ellrott, K. *et al.* Scalable Open Science Approach for Mutation Calling of Tumor Exomes Using Multiple Genomic Pipelines. *Cell Syst* **6**, 271-281.e277, doi:10.1016/j.cels.2018.03.002 (2018).
85 Van der Auwera GA & O'Connor BD. *Genomics in the Cloud: Using Docker, GATK, and WDL in Terra (1st Edition).* O'Reilly Media, (2020).
86 Koboldt, D. C., Larson, D. E. & Wilson, R. K. Using VarScan 2 for Germline Variant Calling and Somatic Mutation Detection. *Curr Protoc Bioinformatics* **44**, 15.14.11-17, doi:10.1002/0471250953.bi1504s44 (2013).
87 Kim, S. *et al.* Strelka2: fast and accurate calling of germline and somatic variants. *Nat Methods* **15**, 591-594, doi:10.1038/s41592-018-0051-x (2018).
88 Fan, Y. *et al.* MuSE: accounting for tumor heterogeneity using a sample-specific error model improves sensitivity and specificity in mutation calling from sequencing data. *Genome Biol* **17**, 178, doi:10.1186/s13059-016-1029-6 (2016).
89 McLaren, W. *et al.* The Ensembl Variant Effect Predictor. *Genome Biol* **17**, 122, doi:10.1186/s13059-016-0974-4 (2016).
90 Shen, R. & Seshan, V. E. FACETS: allele-specific copy number and clonal heterogeneity analysis tool for high-throughput DNA sequencing. *Nucleic Acids Res* **44**, e131, doi:10.1093/nar/gkw520 (2016).
91 Bergstrom, E. N. *et al.* SigProfilerMatrixGenerator: a tool for visualizing and exploring patterns of small mutational events. *BMC Genomics* **20**, 685, doi:10.1186/s12864-019-6041-2 (2019).
92 Bergstrom, E. N., Barnes, M., Martincorena, I. & Alexandrov, L. B. Generating realistic null hypothesis of cancer mutational landscapes using SigProfilerSimulator. *BMC Bioinformatics* **21**, 438, doi:10.1186/s12859-020-03772-3 (2020).
93 Bergstrom, E. N., Kundu, M., Tbeileh, N. & Alexandrov, L. B. Examining clustered somatic mutations with SigProfilerClusters. *Bioinformatics* **38**, 3470-3473, doi:10.1093/bioinformatics/btac335 (2022).
94 S.M. Ashiqul Islam, M. D.-G., Yang Wu, Mark Barnes, Raviteja Vangara, Erik N. Bergstrom, Yudou He, Mike Vella, Jingwei Wang, Jon W. Teague, Peter Clapham, Sarah Moody, Sergey Senkin, Yun Rose Li, Laura Riva, Tongwu Zhang, Andreas J. Gruber, Christopher D. Steele, Burçak Otlu, Azhar Khandekar, Ammal Abbasi, Laura Humphreys, Natalia Syulyukina, Samuel W. Brady, Boian S. Alexandrov, Nischalan Pillay, Jinghui Zhang, David J. Adams, Iñigo Martincorena, David C. Wedge, Maria Teresa Landi, Paul Brennan, Michael R. Stratton, Steven G. Rozen, Ludmil B. Alexandrov. Uncovering novel mutational signatures by de novo extraction with SigProfilerExtractor. *Cell Genomics* **Volume 2**, doi:https://doi.org/10.1016/j.xgen.2022.100179 (2022).
95 Thorvaldsdóttir, H., Robinson, J. T. & Mesirov, J. P. Integrative Genomics Viewer (IGV): high-performance genomics data visualization and exploration. *Brief Bioinform* **14**, 178-192, doi:10.1093/bib/bbs017 (2013).
96 Gu, Z., Eils, R. & Schlesner, M. Complex heatmaps reveal patterns and correlations in multidimensional genomic data. *Bioinformatics* **32**, 2847-2849, doi:10.1093/bioinformatics/btw313 (2016).
97 Gu, Z., Gu, L., Eils, R., Schlesner, M. & Brors, B. circlize Implements and enhances circular visualization in R. *Bioinformatics* **30**, 2811-2812, doi:10.1093/bioinformatics/btu393 (2014).

98 Günther, F., Dudschig, C. & Kaup, B. LSAfun--An R package for computations based on Latent Semantic Analysis. *Behav Res Methods* **47**, 930-944, doi:10.3758/s13428-014-0529-0 (2015).

ACKNOWLEDGEMENTS

The authors would like to thank Dr. John Murray (Indiana University Bloomington) for providing human foreskin fibroblasts. This work was supported by an Alfred P. Sloan Research Fellowship to LBA. LBA is also an Abeloff V scholar, and he is personally supported by a Packard Fellowship for Science and Engineering. This work was also supported by the US National Institute of Health grants R01ES030993-01A1, R01ES032547-01, and R01CA269919-01 to LBA as well as R35ES031638-03 to BVH. The funders had no roles in study design, data collection and analysis, decision to publish, or preparation of the manuscript.

AUTHOR CONTRIBUTIONS

LBA and MZ designed all experiments with help from BVH. MZ performed all experiments with assistance from AH, NV, SPN and YY. MZ performed all data analysis with help from CY, JD, BO, and YH. BVH assisted in the writing of the manuscript and helped interpreting the experimental results. The manuscript was written by LBA and MZ with input from all other authors. LBA supervised the overall project and writing of the manuscript. All authors read and approved the final manuscript.

COMPETING INTERESTS

LBA is a compensated consultant and has equity interest in io9, LLC. All other authors declare no competing interests.

971 **FIGURE LEGENDS**

972 **Figure 1. Overview of the overall study design.** ***(a)*** Primary mammalian cells, MEFs and HFFs,
973 were expanded into 6-well plates and treated with ultraviolet light (UV) emitted from a UV-nail
974 polish dryer for 20 minutes, twice a day within one single day, termed *acute UV exposure*. For
975 *chronic UV exposure*, primary cells were exposed consecutively in three different days with each
976 exposure lasting 20 minutes. Control samples were maintained in the dark in pre-warmed PBS for
977 20 minutes during each exposure session. After recovery and cellular selection, whether through
978 senescence bypass or single-cell subcloning, control and irradiated cell were grown for the same
979 number of doubling populations and subjected to bulk whole-genome sequencing. Analysis of
980 whole-genome sequenced samples was performed using our established pipelines for mutation
981 calling. Analysis of mutational signatures was performed using the SigProfiler suite of tools. ***(b)***
982 Primary HEKa cells were irradiated in 10-cm dishes using UV-nail polish dryer for 20 minutes for
983 three consecutive days. Control samples were maintained in the dark in pre-warmed PBS for 20
984 minutes during each exposure session. HEKa cells were kept in culture for 14 days for recovery
985 and replication, allowing around 8 doubling-populations after which the cells were subjected to
986 high coverage duplex sequencing. Analysis of duplex sequencing samples was performed using
987 commercially established pipelines. Analysis of mutational signatures was performed using the
988 SigProfiler suite of tools. Asterisks in panels *(a)* and *(b)* denote timepoints when DNA damage
989 and other assessments were performed for each condition, including interrogation of cytotoxicity,
990 genotoxicity, oxidative damage, and mitochondrial damage (**Supplementary Table 1**).

991

992 **Figure 2. Cytotoxicity and genotoxicity in mammalian cells after irradiation with a UV-nail**
993 **dryer.** ***(a)*** Cytotoxicity assessment following exposure of primary MEFs (top panel), HFFs

994 (middle panel), and HEKa (bottom panel) to UV radiation emitted from a UV-nail polish dryer for
995 different timepoints, ranging from 0 to 20 minutes. Multiple UV-exposure sessions were tested
996 with one hour difference between each consecutive exposure, including: grey – one exposure in a
997 day; yellow – two exposures in a day; red – three exposures in a day. Formazan dye absorbance
998 was measured 48 hours after treatment cessation and was normalized to the number of unirradiated
999 control cells at timepoint 0. The results are presented as mean percentage ± standard deviation
1000 from at least four replicates (n=4 for MEFs, n=5 for HFFs, n=4 for HEKa). Statistically significant
1001 results from FDR corrected Mann-Whitney U two-sided tests are denoted as: *q-value<0.05. ***(b)***
1002 DNA damage evaluation by immunofluorescence of Ser139-pjosphorylated histone H2Ax
1003 (γH2Ax). Primary MEFs (top panel), HFFs (middle panel) and HEKa (bottom panel), were
1004 exposed to UV radiation either acutely or chronically. DAPI is shown in blue, Phalloidin in red,
1005 and γH2Ax in green. ***(c-e)*** Quantification of the number of γH2Ax foci was performed by analyzing
1006 100 cells per condition, collected from at least 3 independent experiments, in MEF (n=4) ***(c)***, HFF
1007 (n=3) ***(d)*** and HEKa (n=3) ***(e)*** cells. The bounds of the boxplots represent the interquartile range
1008 divided by the median, and Tukey-style whiskers extend to a maximum of 1.5 × interquartile range
1009 beyond the box. Statistically significant results from FDR corrected Mann-Whitney U two-sided
1010 tests are denoted as q-values.
1011
1012 **Figure 3. Oxidative damage in mammalian cells after irradiation with a UV-nail dryer. (*a*)**
1013 Assessment of oxidative DNA damage by live imaging of CellROX green reagent in control and
1014 irradiated MEF (top panel), HFF (middle panel), and HEKa (bottom panel) cells. DAPI is shown
1015 in blue while CellROX is shown in green. ***(b)*** HEKa cells were challenged with 2mM N-acetyl-L-
1016 cysteine (NAC) for 1 hour prior to irradiation. Quantification of the number of CellROX foci was

1017 performed by analyzing at least 100 cells per condition and comparing cells with and without NAC
1018 pre-treatment, collected from triplicates. The bounds of the boxplots represent the interquartile
1019 range divided by the median, and Tukey-style whiskers extend to a maximum of 1.5 × interquartile
1020 range beyond the box. ***(c-e)*** Oxidative DNA damage measurement of 8-oxo-7,8-dihydro-2′-
1021 deoxyguanosine (8-oxo-dG) by ELISA in MEF ***(c)***, HFF ***(d)***, and HEKa ***(e)*** cells. Measurements
1022 of 8-oxo-dG were performed at different timepoints (0, 4, 24 hours post-treatment). Measurements
1023 of 8-oxo-dG were also performed on a negative control (NC), consisting of water only, and on
1024 three positive controls, namely, hydrogen peroxide (H_2O_2), ultraviolet C radiation (UVC), and
1025 potassium bromate ($KBrO_3$). In all cases, data are presented as a mean value ± standard deviation
1026 from *n=3* independent biological replicates. For all panels: statistically significant results from
1027 FDR corrected Mann-Whitney U two-sided tests are denoted as: *q-value<0.05; **q-value<0.01;
1028 ***q-value<0.001; and ****q-value<0.0001.
1029
1030 **Figure 4. Mitochondrial disruption after irradiation with a UV-nail dryer in HEKa cells.** ***(a)***
1031 Evaluating the mitochondrial membrane potential after irradiation of HEKa cells with a UV-nail
1032 dryer. DAPI is shown in blue, MitoTracker in green, and tetramethylrhodamine dye (TMRM) in
1033 red. Yellow corresponds to overlaps between MitoTracker and TMRM. Images collected from
1034 three independent experiments. ***(b)*** Examining mitochondrial ROS production in HEKa cells.
1035 DAPI is shown in blue, MitoTracker in green, and MitoSOX in red. Yellow corresponds to
1036 overlaps between MitoTracker and MitoSOX. In both panels (*a*) and (*b*), MitoTracker green
1037 reagent is used to localize mitochondria regardless of mitochondria membrane potential. Images
1038 collected from three independent experiments. **(*c*)** Quantification of the number of MitoSOX foci
1039 in 100 cells per condition in HEKa, examined over 4 independent replicates. The bounds of the

1040 boxplots represent the interquartile range divided by the median, and Tukey-style whiskers extend
1041 to a maximum of 1.5 × interquartile range beyond the box. Statistically significant results from
1042 FDR corrected Mann-Whitney U two-sided tests are denoted as *q*-values.
1043
1044 **Figure 5. Mutations found in the genomes of MEFs and HFFs irradiated by a UV-nail dryer.**
1045 ***(a)*** Mutation count per megabase (Mb) detected in the different conditions, represented in colors,
1046 in MEFs and HFFs. Data is presented as a mean value ± standard error from *n=5* independent
1047 biological replicates. Statistically significant results from FDR corrected Mann-Whitney U two-
1048 sided tests are denoted as: *q-value<0.05; **q-value<0.01. ***(b)*** Fold-increase of single base
1049 substitutions in UV-treated clones compared to controls. Fold increase is expressed as mean fold-
1050 change ± SE (standard error) from *n=5* independent replicates. ***(c)*** Spearman's rank correlations
1051 between the number of C>A substitutions and the number UV exposures in the five independent
1052 UV-treated clones in MEFs (top panel) and HFFs (bottom panel). Acute and chronic exposures
1053 correspond to 2 and 3 exposures, respectively. P-value is calculated based on a two-sided t-
1054 distribution with n-2 degrees of freedom. Grey bands represent the 95% confidence intervals. ***(d)***
1055 Number of small insertions and deletions (indels) in MEF and HFF clones for each irradiation
1056 condition.
1057
1058 **Figure 6. Mutation analysis of HEKa cells irradiated by a UV-nail dryer.** ***(a)*** Mutation count
1059 per megabase (Mb) detected in the different conditions, represented in colors, in HEKa cells. Data
1060 is presented as a mean value ± standard error from *n=3* independent biological replicates. **(*b*)** Fold-
1061 increase of single base substitutions in UV-treated clones compared to controls. Fold increase is
1062 expressed as mean fold-change ± SE (standard error) from *n=3* independent replicates. ***(c)***

1063 Spearman's rank correlations between the number of C>A substitutions and the number UV
1064 exposures in each of the 3 biological replicates. P-value is calculated based on two-sided t-
1065 distribution with *n-2* degrees of freedom. Grey bands represent the 95% confidence intervals. ***(d)***
1066 Number of small insertions and deletions (indels) in HEKa cells. Statistically significant results
1067 from FDR corrected Mann-Whitney U tests are denoted as: *q-value<0.05; **q-value<0.01; ***q-
1068 value<0.001; and ****q-value<0.0001.
1069
1070 **Figure 7. Somatic Mutations due to COSMIC signatures SBS18/36 in cells and cancer**
1071 **samples.** ***(a)*** The patterns of mutational signatures COSMIC SBS18 and SBS36. ***(b)*** Number of
1072 mutations per megabase attributed to COSMIC SBS18/36 in UV exposed MEF clones, per
1073 condition, extracted from *n=5* biological replicates per condition. **(*c*)** Number of mutation per
1074 megabase attributed to COSMIC SBS18/36 in UV exposed HFF clones, per condition, extracted
1075 from *n=5* biological replicates per condition. **(*d*)** Mutational patterns of irradiated (upper track)
1076 and control (lower track) primary HEKa cells. **(*e*)** COSMIC signatures assignment of UV-
1077 irradiated HEKa cells (upper track) and control (lower track). **(*f*)** Pearson's correlation of C>A and
1078 C>T mutations in *n=144* skin cancer samples from the PCAWG project. P-value is calculated
1079 based on two-sided t-distribution with *n-2* degrees of freedom. The bounds of the boxplots
1080 represent the interquartile range divided by the median, and Tukey-style whiskers extend to a
1081 maximum of 1.5 × interquartile range beyond the box.

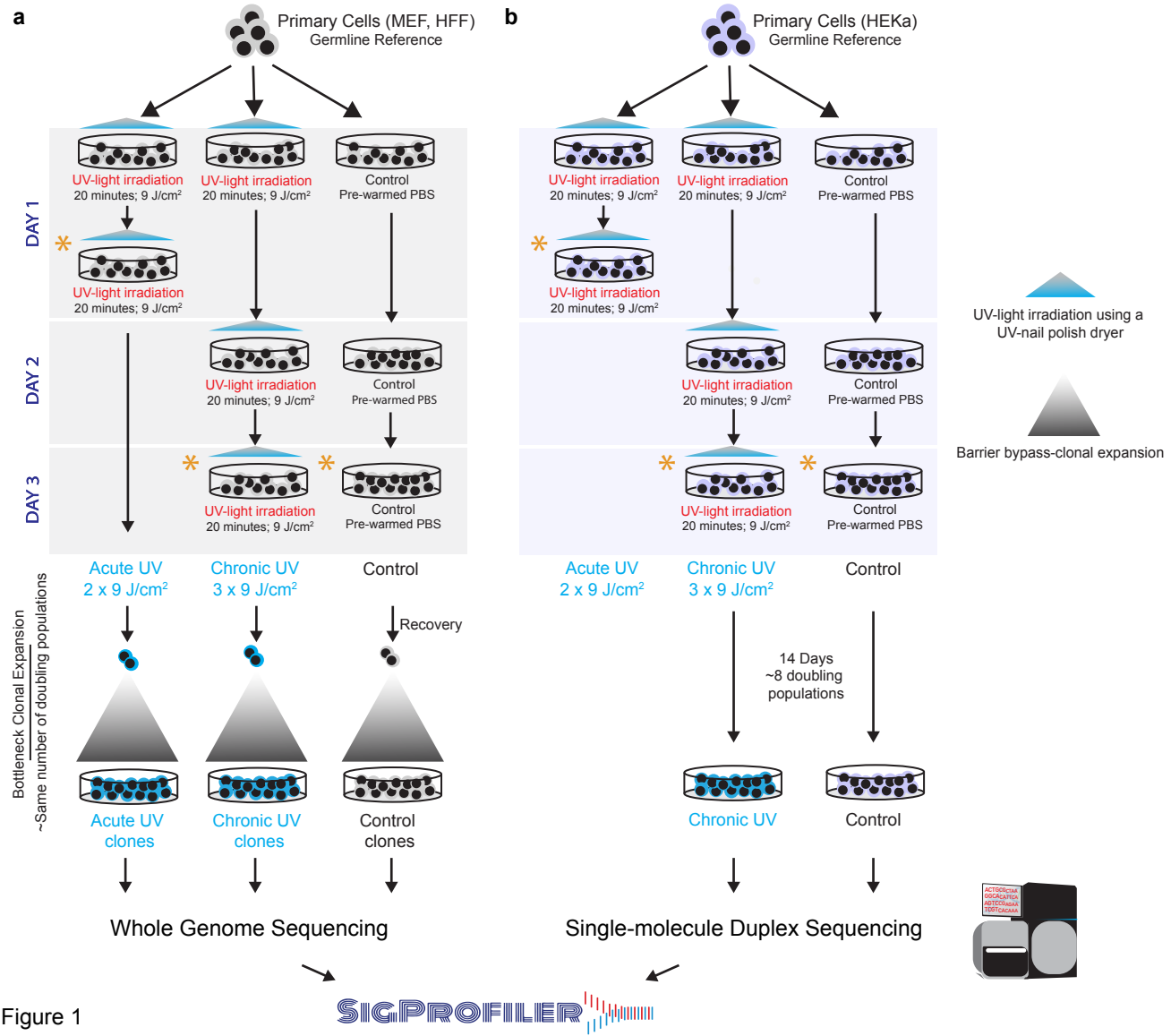
a
Primary Cells (MEF, HFF)
Germline Reference
UV-light irradiation
20 minutes; 9 J/cm²
Control
Pre-warmed PBS
DAY 1
DAY 2
DAY 3
Acute UV
2 x 9 J/cm²
Chronic UV
3 x 9 J/cm²
Control
Recovery
Bottleneck Clonal Expansion
~Same number of doubling populations
Acute UV clones
Chronic UV clones
Control clones
Whole Genome Sequencing
b
Primary Cells (HEKa)
Germline Reference
14 Days
~8 doubling populations
Chronic UV
Control
Single-molecule Duplex Sequencing
UV-light irradiation using a UV-nail polish dryer
Barrier bypass-clonal expansion
SIGPROFILER

Figure 1

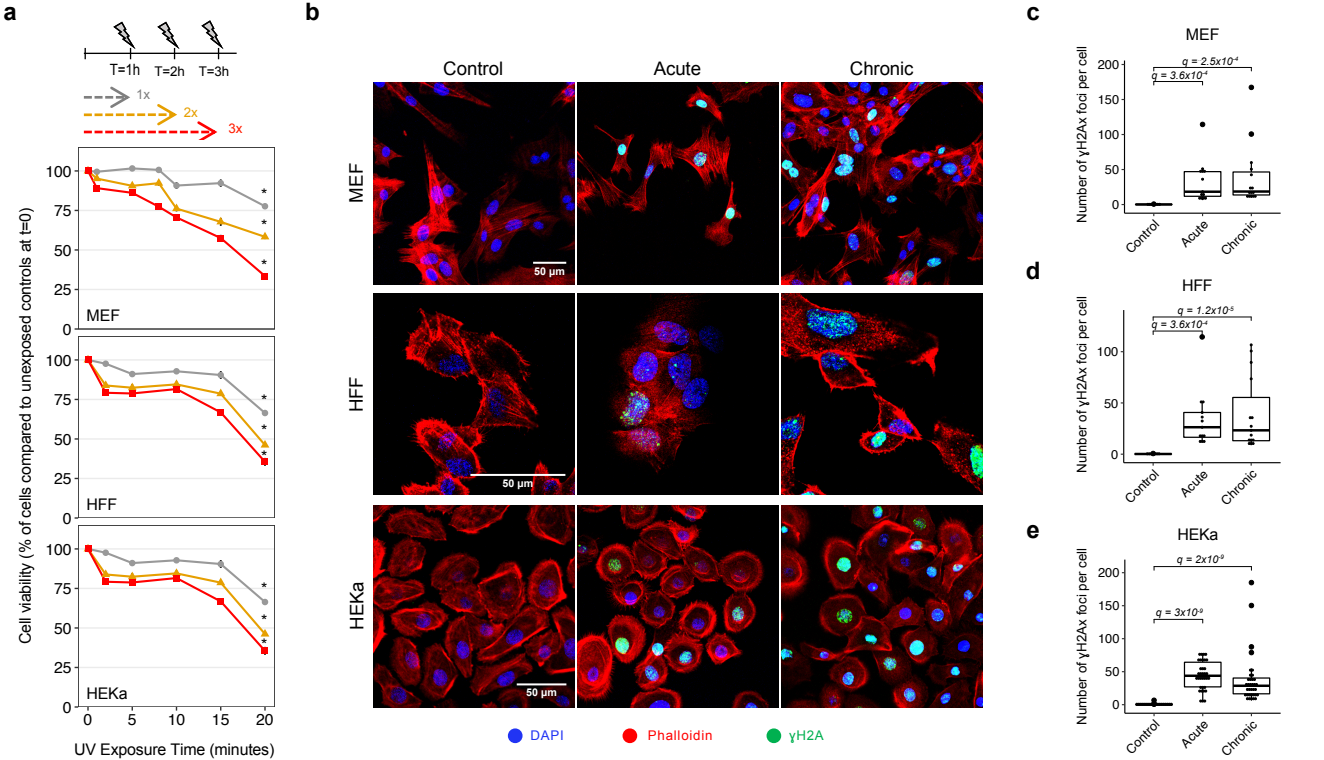
a
T=1h
T=2h
T=3h
1x
2x
3x
Cell viability (% of cells compared to unexposed controls at t=0)
MEF
HFF
HEKa
UV Exposure Time (minutes)
b
Control
Acute
Chronic
MEF
HFF
HEKa
50 µm
DAPI
Phalloidin
γH2A
c
MEF
q = 2.5x10-4
q = 3.6x10-4
Number of γH2Ax foci per cell
Control
Acute
Chronic
d
HFF
q = 1.2x10-5
q = 3.6x10-4
e
HEKa
q = 2x10-9
q = 3x10-9

Figure 2

Figure 3

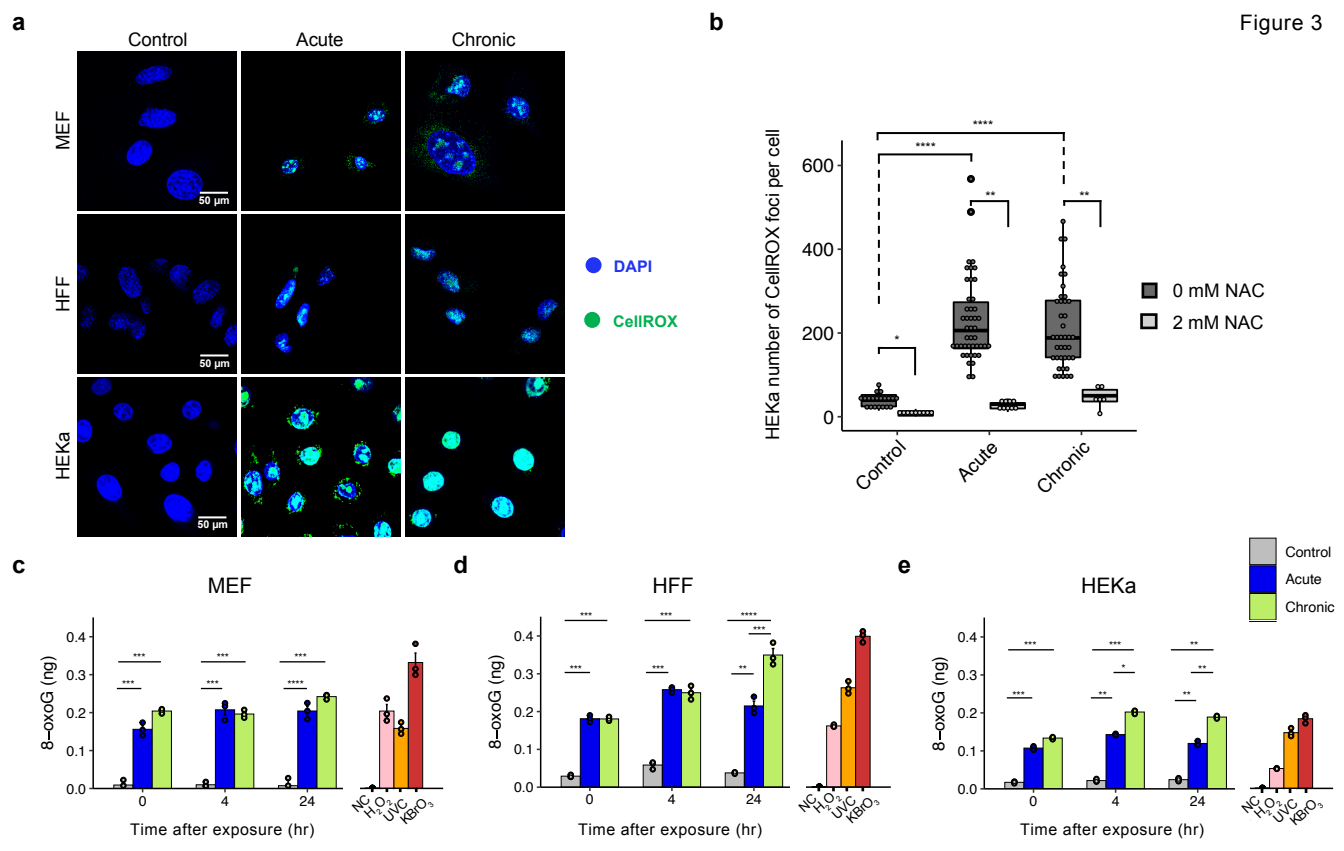
a
Control
Acute
Chronic
MEF
HFF
HEKa
50 µm
DAPI
CellROX
b
HEKa number of CellROX foci per cell
0 mM NAC
2 mM NAC
Control
Acute
Chronic
c
MEF
d
HFF
e
HEKa
8–oxoG (ng)
Time after exposure (hr)
NC
H_2O_2
UVC
$KBrO_3$
Control
Acute
Chronic

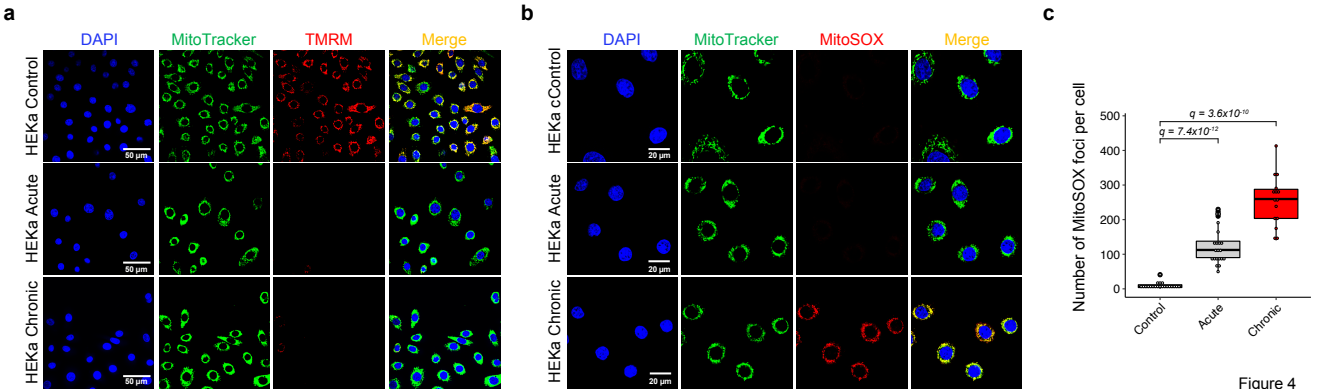
a
DAPI
MitoTracker
TMRM
Merge
HEKa Control
HEKa Acute
HEKa Chronic
50 µm
b
DAPI
MitoTracker
MitoSOX
Merge
HEKa cControl
HEKa Acute
HEKa Chronic
20 µm
c
Number of MitoSOX foci per cell
q = 3.6x10-10
q = 7.4x10-12
500
400
300
200
100
0
Control
Acute
Chronic

Figure 4

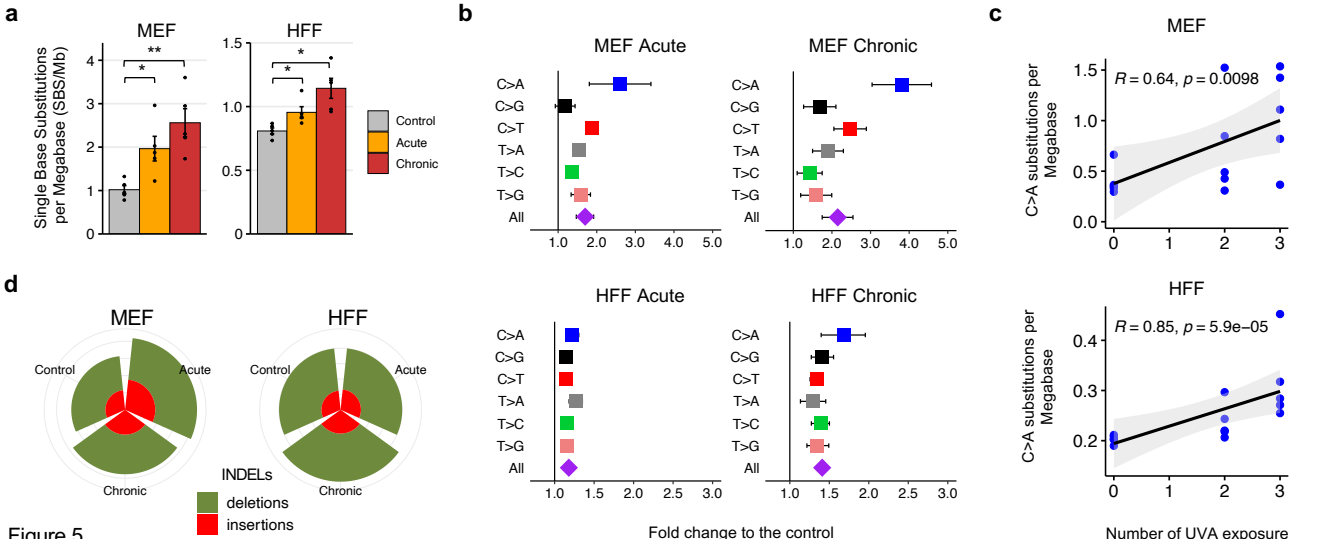
a
MEF
HFF
Single Base Substitutions per Megabase (SBS/Mb)
Control
Acute
Chronic
b
MEF Acute
MEF Chronic
HFF Acute
HFF Chronic
C>A
C>G
C>T
T>A
T>C
T>G
All
Fold change to the control
c
MEF
HFF
C>A substitutions per Megabase
R = 0.64, p = 0.0098
R = 0.85, p = 5.9e−05
Number of UVA exposure
d
MEF
HFF
Control
Acute
Chronic
INDELs
deletions
insertions

Figure 5

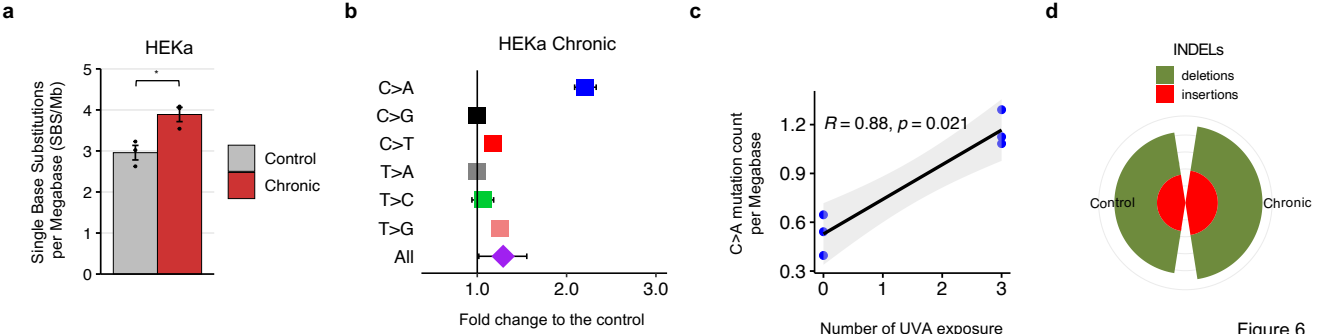
a
HEKa
Single Base Substitutions per Megabase (SBS/Mb)
5
4
3
2
1
0
*
Control
Chronic
b
HEKa Chronic
C>A
C>G
C>T
T>A
T>C
T>G
All
1.0
2.0
3.0
Fold change to the control
c
R = 0.88, p = 0.021
C>A mutation count per Megabase
1.2
0.9
0.6
0.3
0
1
2
3
Number of UVA exposure
d
INDELs
deletions
insertions
Control
Chronic

Figure 6

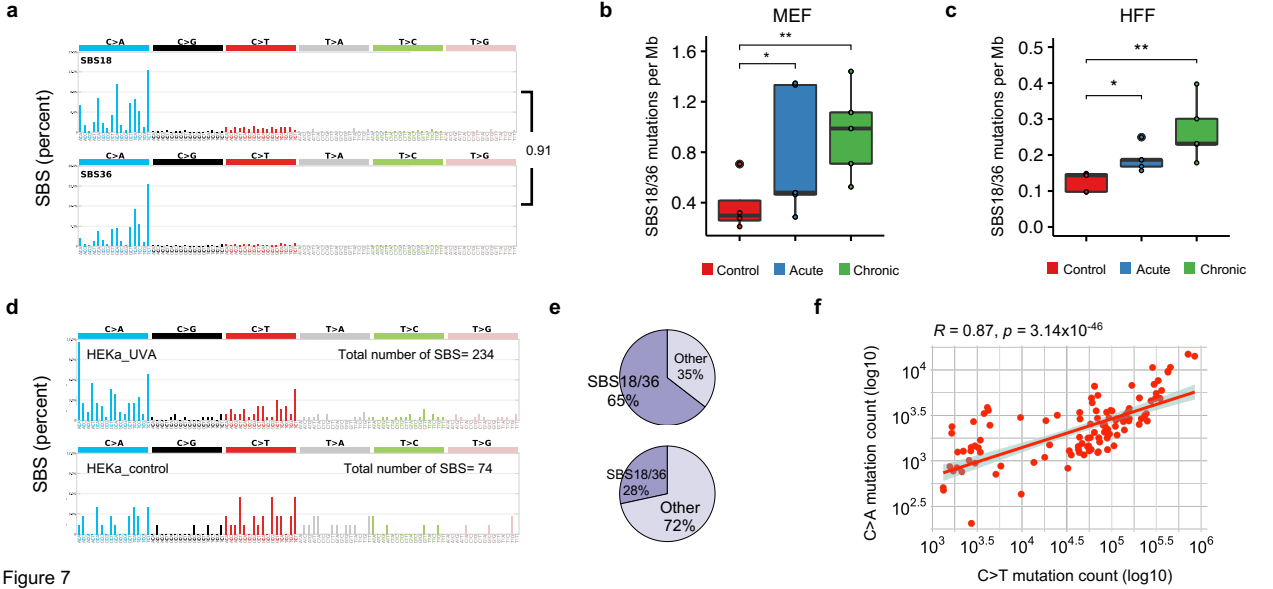
a
C>A
C>G
C>T
T>A
T>C
T>G
SBS18
SBS36
SBS (percent)
0.91
b
MEF
SBS18/36 mutations per Mb
1.6
1.2
0.8
0.4
*
**
Control
Acute
Chronic
c
HFF
SBS18/36 mutations per Mb
0.5
0.4
0.3
0.2
0.1
0.0
*
**
Control
Acute
Chronic
d
HEKa_UVA
Total number of SBS= 234
HEKa_control
Total number of SBS= 74
SBS (percent)
e
SBS18/36
65%
Other
35%
SBS18/36
28%
Other
72%
f
R = 0.87, p = 3.14x10-46
C>A mutation count (log10)
C>T mutation count (log10)
10^4
10^3.5
10^3
10^2.5
10^3
10^3.5
10^4
10^4.5
10^5
10^5.5
10^6

Figure 7